GE Nuclear Energy

# AN ASME SECTION VIII EVALUATION OF THE OYSTER CREEK DRYWELL FOR WITHOUT SAND CASE PART 2 STABILITY ANALYSIS (Revision 2)

November 1992

prepared for

GPU Nuclear Corporation
Parsippany, New Jersey

prepared by

GE Nuclear Energy
San Jose, California

# AN ASME SECTION VIII EVALUATION OF THE OYSTER CREEK DRYWELL FOR WITHOUT SAND CASE PART 2 STABILITY ANALYSIS (Revision 2)

Prepared by: _____

M.L.Herrera, Senior Engineer
Materials Monitoring &
Structural Analysis Services

Verified by: _____

H. S. Mehta, Principal Engineer
Materials Monitoring &
Structural Analysis Services

Approved by: _____

S. Ranganath, Manager
Materials Monitoring &
Structural Analysis Services

TABLE OF CONTENTS

# LIST OF TABLES

LIST OF FIGURES

# LIST OF FIGURES

# 1. INTRODUCTION

## 1.1 General

To address local wall thinning of the Oyster Creek drywell, GPUN has prepared a supplementary report to the Code stress report of record [1-1] which is divided into two parts. Part 1 includes all of the Code stress analysis results other than the buckling capability for the drywell shell [1-2]. Part 2 addresses the buckling capability of the drywell shell shown in Figure 1-1 [1-3]. The supplementary report for the degraded drywell is for the present configuration (with sand support in the lower sphere). One option which is being considered by GPUN to mitigate further corrosion in the sandbed region is to remove the sand. Reference 1-4 and this report evaluate the influence of removing the sand on the code stress analysis and buckling evaluation, respectively. Buckling of the entire drywell shell is considered in this analysis with the sandbed region being the area of primary concern.

## 1.2 Report Outline

Section 2 of this report outlines the methodology used in the buckling capability evaluation. Finite element modeling, analysis and results are described in section 3. Evaluation of the allowable compressive buckling stresses and comparisons with the calculated compressive stresses for the limiting load combinations are covered in section 4. Section 5 presents the summary of results and conclusions.

## 1.3 References

1-1 "Structural Design of the Pressure Suppression Containment Vessels," by Chicago Bridge & Iron Co.,Contract # 9-0971, 1965.

1-2 "An ASME Section VIII Evaluation of the Oyster Creek Drywell - Part 1 Stress Analysis," GE Report No. 9-1, DRF# 00664, November 1990, prepared for GPUN.

1-3 "An ASME Section VIII Evaluation of the Oyster Creek Drywell - Part 2 Stability Analysis," GE Report No. 9-2, DRF# 00664, November 1990, prepared for GPUN.

1-4 "An ASME Section VIII Evaluation of the Oyster Creek Drywell - Part 1 Stress Analysis," GE Report No. 9-3, DRF# 00664, February 1991, prepared for GPUN.

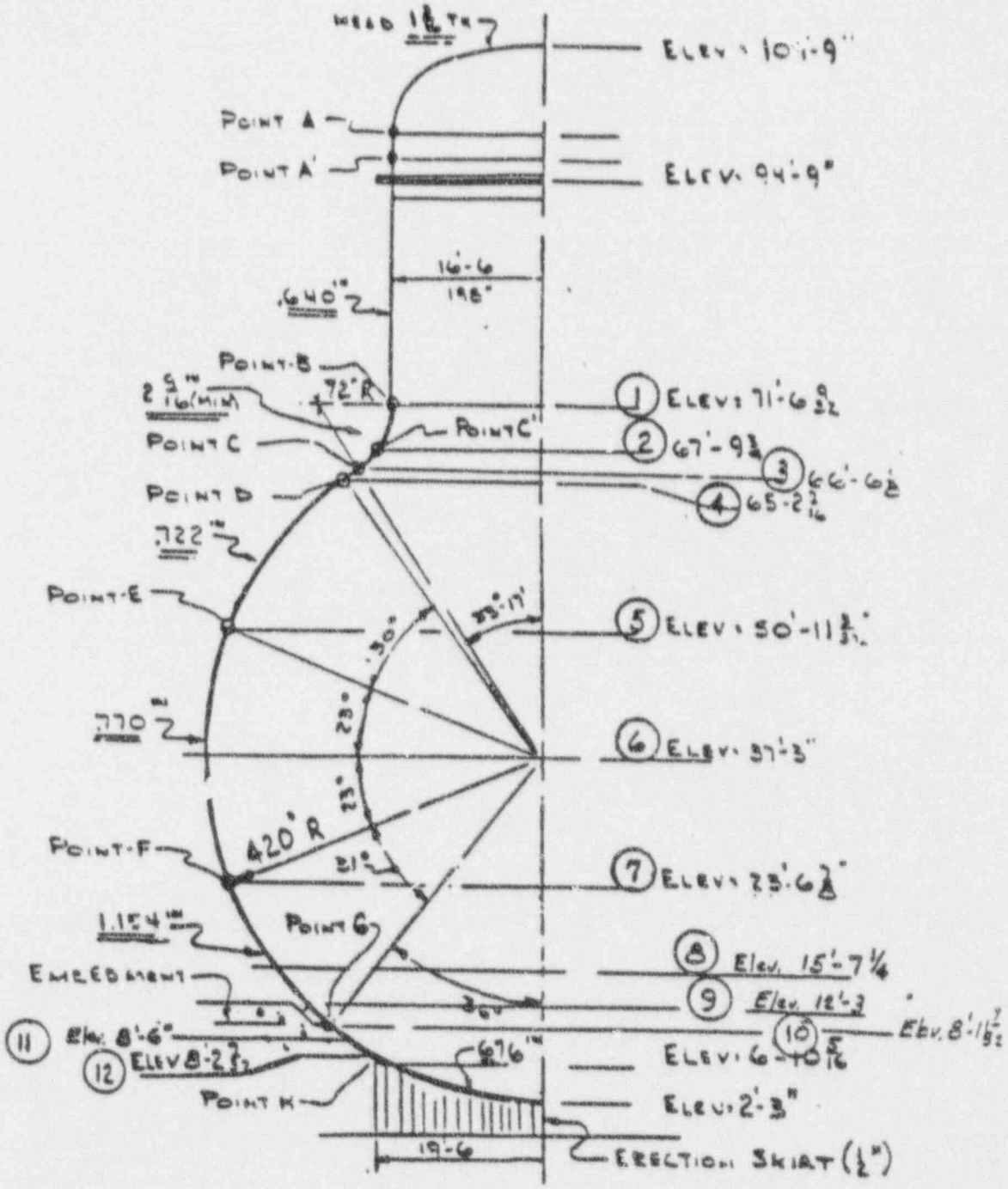


Figure 1-1 Drywell Configuration

# 2. BUCKLING ANALYSIS METHODOLOGY

## 2.1 Basic Approach

The basic approach used in the buckling evaluation follows the methodology outlined in the ASME Code Case N-284 [2-1 and 2-2]. Following the procedure of this Code Case, the allowable compressive stress is evaluated in three steps.

In the first step, a theoretical elastic buckling stress, $\sigma_{ie}$, is determined. This value may be calculated either by classical buckling equations or by finite element analysis. Since the drywell shell geometry is complex, a three dimensional finite element analysis approach is followed using the eigenvalue extraction technique. More details on the eigenvalue determination are given in Section 3.

In the second step, the theoretical elastic buckling stress is modified by the appropriate capacity and plasticity reduction factors. The capacity reduction factor, $\alpha_i$, accounts for the difference between classical buckling theory and actual tested buckling stresses for fabricated shells. This difference is due to imperfections inherent in fabricated shells, not accounted for in classical buckling theory, which can cause significant reductions in the critical buckling stress. Thus, the elastic buckling stress for fabricated shells is given by the product of the theoretical elastic buckling stress and the capacity reduction factor, i.e., $\sigma_{ie}\alpha_i$. When the elastic buckling stress exceeds the proportional limit of the material, a plasticity reduction factor, $\eta_i$, is used to account for non-linear material behavior. The inelastic buckling stress for fabricated shells is given by $\eta_i\alpha_i\sigma_{ie}$.

In the final step, the allowable compressive stress is obtained by dividing the buckling stress calculated in the second step by the safety factor, FS:

$$\text{Allowable Compressive Stress} = \eta_i\alpha_i\sigma_{ie}/FS$$

In Reference 2-1, the safety factor for the Design and Level A & B service conditions is specified as 2.0. A safety factor of 1.67 is specified for Level C service conditions (such as the post-accident condition).

The determination of appropriate values for capacity and plasticity reduction factors is discussed next.

## 2.2 Determination of Capacity Reduction Factor

The capacity reduction factor, $\alpha_j$, is used to account for reductions in actual buckling strength due to the existence of geometric imperfections. The capacity reduction factors given in Reference 2-1 are based on extensive data compiled by Miller [2-3]. The factors appropriate for a spherical shell geometry such as that of the drywell in the sandbed region, are shown in Figure 2-1 (Figure 1512-1 of Reference 2-1). The tail (flat) end of the curves are used for unstiffened shells. The curve marked 'Uniaxial compression' is applicable since the stress state in the sandbed region is compressive in the meridional direction but tensile in the circumferential direction. From this curve, $\alpha_j$ is determined to be 0.207.

The preceding value of the capacity reduction factor is very conservative for two reasons. First, it is based on the assumption that the spherical shell has a uniform thickness equal to the reduced thickness. However, the drywell shell has a greater thickness above the sandbed region which would reinforce the sandbed region. Second, it is assumed that the circumferential stress is zero. The tensile circumferential stress has the effect of rounding the shell and reducing the effect of imperfections introduced during the fabrication and construction phase. A modification of the $\alpha_j$ value to account for the presence of tensile circumferential stress is discussed in Subsection 2.3.

The capacity reduction factor values given in Reference 2-1 are applicable to shells which meet the tolerance requirements of NE-4220

of Section III [2-4]. Reference 2-5 compares the tolerance requirements of NE-4220 to the requirements to which the Oyster Creek drywell shell was fabricated. The comparison shows that the Oyster Creek drywell shell was erected to the tolerance requirements of NE-4220. Therefore, although the Oyster Creek drywell is not a Section III, NE vessel, it is justified to use the approach outlined in Code Case N-284.

## 2.3 Modification of Capacity Reduction Factor for Hoop Stress

The orthogonal tensile stress has the effect of rounding fabricated shells and reducing the effect of imperfections on the buckling strength. The Code Case N-284 [2-1 and 2-2] notes in the last paragraph of Article 1500 that, "The influence of internal pressure on a shell structure may reduce the initial imperfections and therefore higher values of capacity reduction factors may be acceptable. Justification for higher values of $\alpha_i$ must be given in the Design report."

The effect of hoop tensile stress on the buckling strength of cylinders has been extensivelly documented [2-6 through 2-11]. Since the methods used in accounting for the effect of tensile hoop stress for the cylinders and spheres are similar, the test data and the methods for the cylinders are first reviewed. Harris, et al [2-6] presented a comprehensive set of test data, including those from References 2-7 and 2-8, which clearly showed that internal pressure in the form of hoop tension, increases the axial buckling stress of cylinders. Figure 2-2 shows a plot of the test data showing the increase in buckling stress as a function of nondimensional pressure. This increase in buckling capacity is accounted for by defining a separate reduction factor, $\alpha_p$. The capacity reduction factor $\alpha_i$ can then be modified as follows:

$$\alpha_{i,mod} = \alpha_i + \alpha_p$$

The buckling stress in uniaxial compression for a cylinder or a sphere of uniform thickness with no internal pressure is given by the following:

$$S_c = (0.605)(\alpha_i)Et/R$$
$$= (0.605)(0.207)\ Et/R$$

Where, 0.605 is a constant, 0.207 is the capacity reduction factor, $\alpha_i$, and E,t and R are Young's Modulus, wall thickness and radius, respectively. In the presence of a tensile stress such as that produced by an internal pressure, the buckling stress is given as follows:

$$S_{c,mod} = (0.605)(\alpha_i + \alpha_p)Et/R$$
$$= (0.605)(0.207 + \alpha_p)Et/R$$
$$= [(0.605)(0.207) + \Delta C]\ Et/R$$

Where $\Delta C$ is $\alpha_p/0.605$ and is given for cylindrical geometries in the graphical form in Figure 2-3. As can be seen in Figure 2-3, $\Delta C$ is a function of the parameter $X=(p/4E)(2R/t)^2$, where ,p, is the internal pressure. Miller [2-12] gives the following equation that fits the graphical relationship between X and $\Delta C$ shown in Figure 2-3:

$$\Delta C = \alpha_p/0.605 = 1.25/(5+1/X)$$

The preceding approach pertains to cylinders. Along the similar lines, Miller [2-13] has developed an approach for spheres as described next.

The non-dimensional parameter X is essentially $(\sigma_\theta/E)(R/t)$. Since in the case of a sphere, the hoop stress is one-half of that in the cylinder, the parameter X is redefined for spheres as follows:

$$X_{(sphere)} = (p/8E)(2R/t)^2$$

When the tensile stress magnitude, S, is known, the equivalent internal pressure can be calculated using the expression:

$$p = 2tS/R$$

Based on a review of spherical shell buckling data [2-14, 2-15], Miller [2-13] proposed the following equation for $\Delta C$:

$$\Delta C_{(sphere)} = 1.06/(3.24 + 1/X)$$

The modified capacity reduction factor, $\alpha_{i,mod}$, for the drywell geometry was obtained as follows:

$$\alpha_{i,mod} = 0.207 + \Delta C_{(sphere)}/0.605$$

## 2.4 Determination of Plasticity Reduction Factor

When the elastic buckling stress exceeds the proportional limit of the material, a plasticity reduction factor, $\eta_i$, is used to account for the non-linear material behavior. The inelastic buckling stress for fabricated shells is given by $\eta_i\alpha_i\sigma_{ie}$. Reference 2-2 gives the mathematical expressions shown below [Article -1611 (a)] to calculate the plasticity reduction factor for the meridional direction elastic buckling stress. $\Delta$ is equal to $\alpha_i\sigma_{ie}/\sigma_y$ and $\sigma_y$ is the material yield strength. Figure 2-4 shows the relationship in graphical form.

$$\begin{aligned} \eta_i &= 1.0 && \text{if } \Delta \le 0.55 \\ &= (0.45/\Delta) + 0.18 && \text{if } 0.55 < \Delta \le 1.6 \\ &= 1.31/(1+1.15\Delta) && \text{if } 1.6 < \Delta \le 6.25 \\ &= 1/\Delta && \text{if } \Delta > 6.25 \end{aligned}$$

## 2.5 References

2-1 ASME Boiler and Pressure Vessel Code Case N-284, "Metal Containment Shell Buckling Design Methods, Section III, Division 1, Class MC", Approved August 25, 1980.

2-2 Letter (1985) from C.D. Miller to P. Raju; Subject: Recommended Revisions to ASME Code Case N-284.

2-3 Miller, C.D., "Commentary on the Metal Containment Shell Buckling Design Methods of the ASME Boiler and Pressure Vessel Code," December 1979.

2-4 ASME Boiler & Pressure Vessel Code, Section III, Nuclear Power Plant Components.

2-5 "Justification for Use of Section III, Subsection NE, Guidance in Evaluating the Oyster Creek Drywell," Appendix A to letter dated December 21, 1990 from H.S. Mehta of GE to S.C. Tumminelli of GPUN.

2-6 Harris, L.A., et al, "The Stability of Thin-Walled Unstiffened Circular Cylinders Under Axial Compression Including the Effects of Internal Pressure," Journal of the Aeronautical Sciences, Vol. 24, No. 8 (August 1957), pp. 587-596.

2-7 Lo, H., Crate, H., and Schwartz, E.B., "Buckling of Thin-Walled Cylinder Under Axial Compression and Internal Pressure," NACA TN 2021, January 1950.

2-8 Fung, Y.C., and Sechler, E.E., "Buckling of Thin-Walled Circular Cylinders Under Axial Compression and Internal Pressure," Journal of the Aeronautical Sciences, Vol. 24, No. 5, pp. 351-356, May 1957.

2-9 Baker, E.H., et al., "Shell Analysis Manual," NASA, CR-912 (April 1968).

2-10 Bushnell, D., "Computerized Buckling Analysis of Shells," Kluwer Academic Publishers, 1989 (Chapter 5).

2-11 Johnson, B.G., "Guide to Stability Design Criteria for Metal Structures," Third Edition (1976), John Wiley & Sons.

2-12 Miller, C.D., "Effects of Internal Pressure on Axial Compression Strength of Cylinders," CBI Technical Report No. 022891, February 1991.

2-13 Miller, C.D., "Evaluation of Stability Analysis Methods Used for the Oyster Creek Drywell," CBI Technical Report Prepared for GPU Nuclear Corporation, September 1991.

2-14 Odland, J., "Theoretical and Experimental Buckling Loads of Imperfect Spherical Shell Segments," Journal of Ship Research, Vol. 25, No.3, September 1981, pp. 201-218.

2-15 Yao, J.C., "Buckling of a Truncated Hemisphere Under Axial Tension," AIAA Journal, Vol. 1, No. 10, October 1963, pp. 2316-2319.

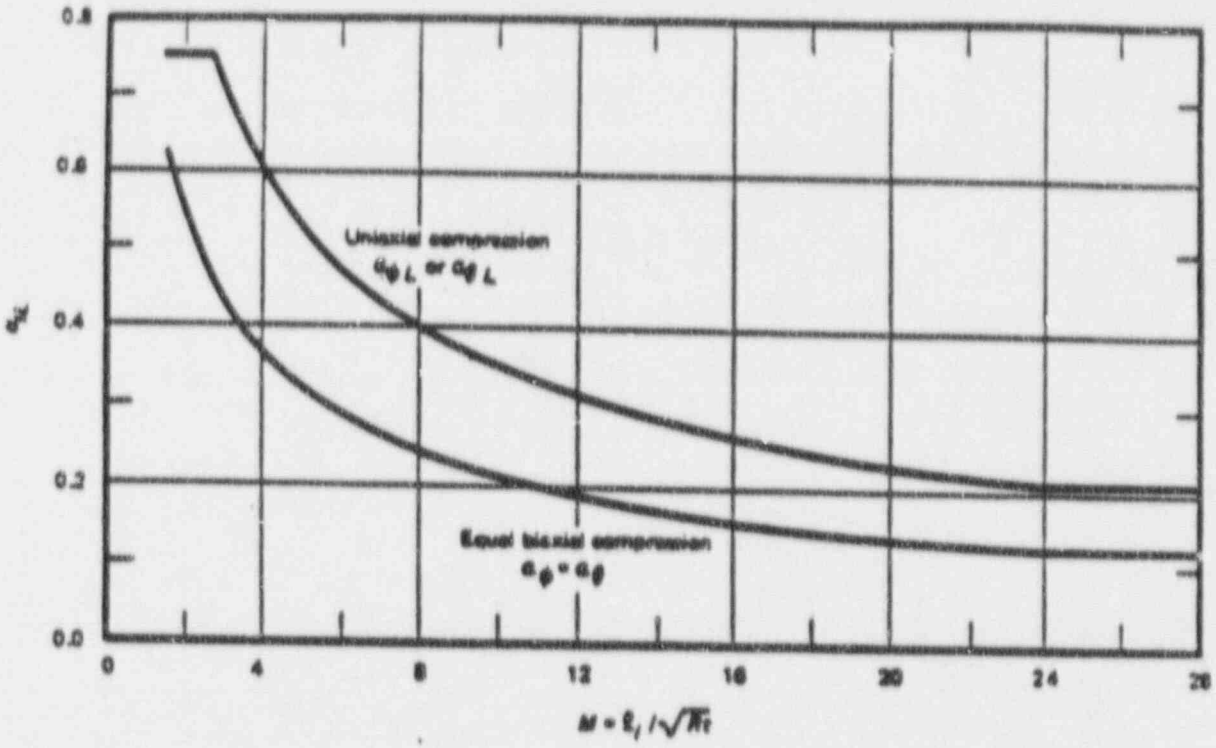


Figure 2-1 Capacity Reduction Factors for Local Buckling of Stiffened and Unstiffened Spherical Shells

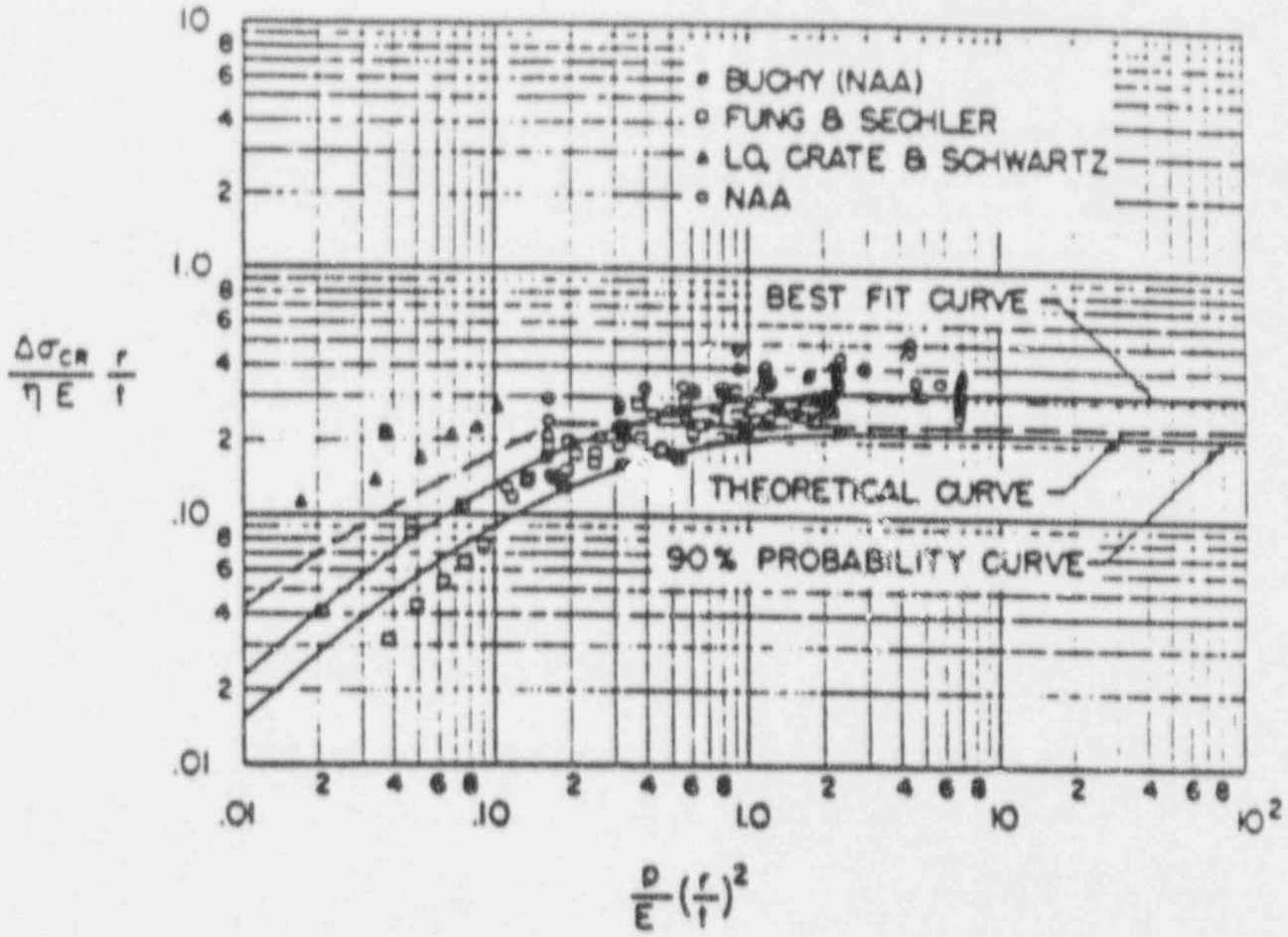


Figure 2-2 Experimental Data Showing Increase in Compressive Buckling Stress Due to Internal Pressure (Reference 2-6)

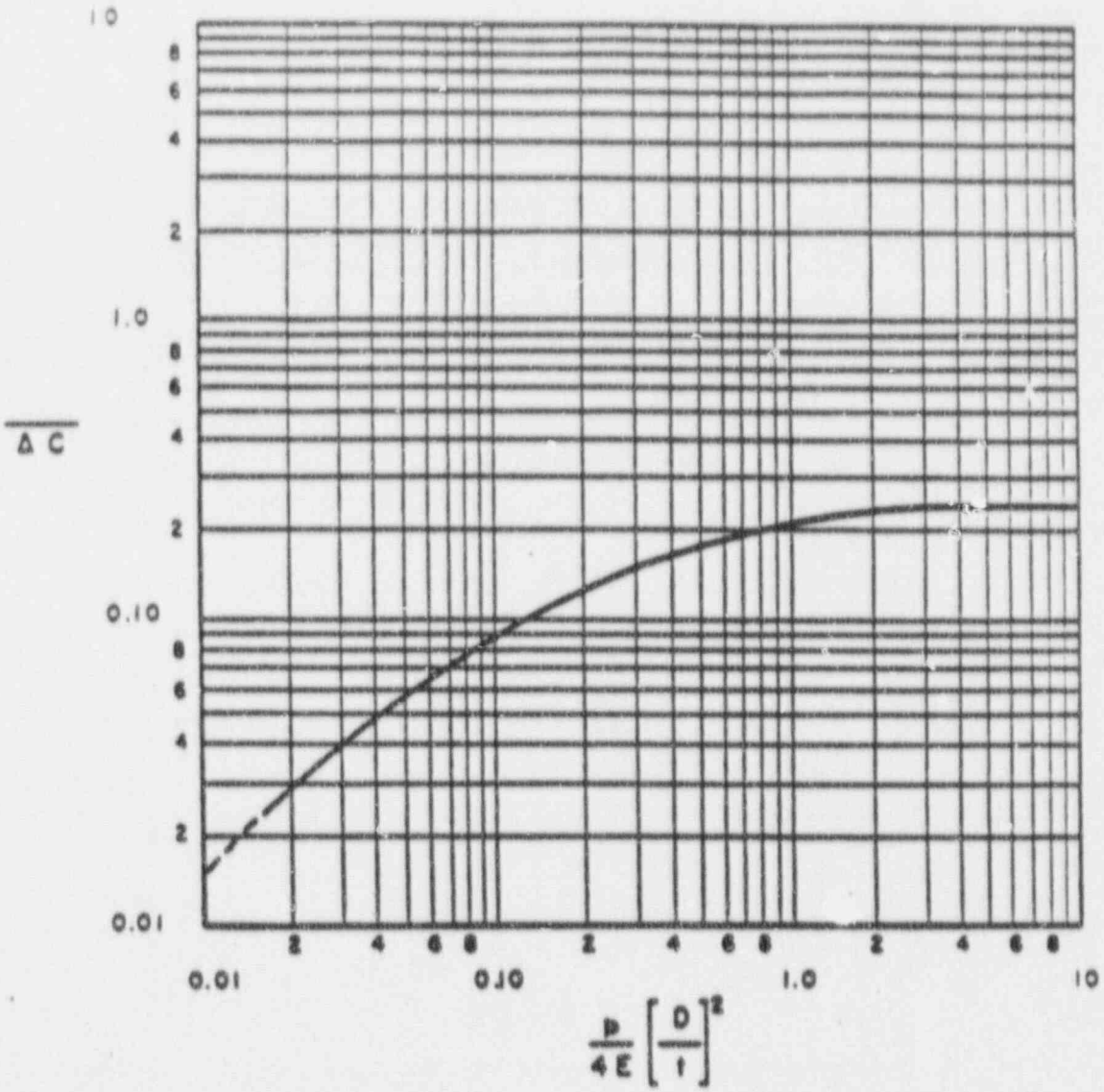


Figure 2-3 Design Curve to Account for Increase in Compressive Buckling Stress Due to Internal Pressure (Reference 2-11)

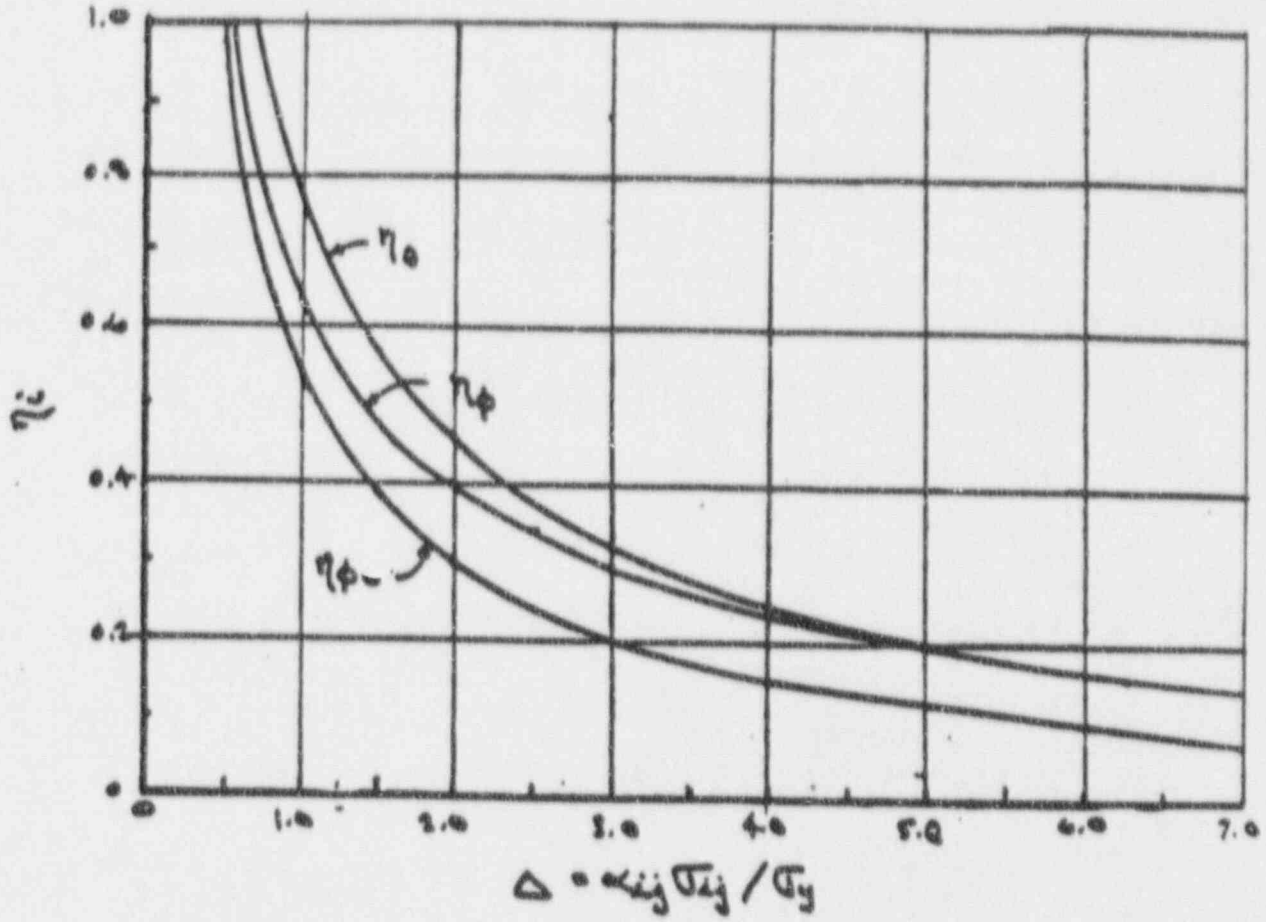


Figure 2-4 Plasticity Reduction Factors for Inelastic Buckling

# 3. FINITE ELEMENT MODELING AND ANALYSIS

## 3.1 Finite Element Buckling Analysis Methodology

This evaluation of the Oyster Creek Drywell buckling capability uses the Finite Element Analysis (FEA) program ANSYS [Reference 3-1]. The ANSYS program uses a two step eigenvalue formulation procedure to perform linear elastic buckling analysis. The first step is a static analysis of the structure with all anticipated loads applied. The structural stiffness matrix, [K], the stress stiffness matrix, [S], and the applied stresses, $\sigma_{ap}$, are developed and saved from this static analysis. A buckling pass is then run to solve for the eigenvalue or load factor, $\lambda$, for which elastic buckling is predicted using the equation:

$$( [K] + \lambda [S] ) (u) = 0$$

where: $\lambda$ is the eigenvalue or load factor.

(u) is the eigenvector representing the buckled shape of the structure.

This load factor is a multiplier for the applied stress state at which the onset of elastic buckling will theoretically occur. All applied loads (pressures, forces, gravity, etc...) are scaled equally. For example, a load factor of 4 would indicate that the structure would buckle for a load condition four times that defined in the stress pass. The critical stress, $\sigma_{cr}$, at a certain location of the structure is thus calculated as:

$$\sigma_{cr} = \lambda \sigma_{ap}$$

This theoretical elastic buckling stress is then modified by the capacity and plasticity reduction factors to determine the predicted buckling stress of the fabricated structure as discussed in Section 2. This stress is further reduced by a factor of safety to determine the allowable compressive stress.

## 3.2 Finite Element Model

The Oyster Creek drywell has been previously analyzed using a simplified axisymmetric model to evaluate the buckling capability in the sandbed region [Reference 3-2]. This type of analysis conservatively neglects the vents and reinforcements around the vents which significantly increase the stiffness of the shell near the sandbed region. In order to more accurately determine the buckling capability of the drywell, a three dimensional finite element model is developed.

The geometry of the Oyster Creek drywell is shown in Figure 3-1. Taking advantage of symmetry of the drywell with 10 vents, a 36° section is modeled. Figure 3-2 illustrates the finite element model of the drywell. This model includes the drywell shell from the base of the sandbed region to the top of the elliptical head and the vent and vent header. The torus is not included in this model because the bellows provide a very flexible connection which does not allow significant structural interaction between the drywell and torus.

Figure 3-3 shows a more detailed view of the lower section of the drywell model. The various colors on Figures 3-2 and 3-3 represent the different shell thicknesses of the drywell and vent. Nominal or as-designed thicknesses, summarized in Table 3-1, are used for the drywell shell for all regions other than the sandbed region. The sandbed region shown in blue in Figure 3-3 is considered to have a thickness of 0.736 inch. This is the 95% confidence projected thickness to outage 14R. Figure 3-4 shows the view from the inside of the drywell with the gussets and the vent jet deflector.

The drywell and vent shell are modeled using the 3-dimensional plastic quadrilateral shell (STIF43) element. Although this element has plastic capabilities, this analysis is conducted using only elastic behavior. This element type was chosen over the elastic quadrilateral shell (STIF63) element because it is better suited for modeling curved surfaces.

At a distance of 76 inches from the drywell shell, the vent is simplified using beam elements. The transition from shell to beam elements is made by extending rigid beam elements from a node along the centerline of the vent radially outward to each of the shell nodes of the vent. ANSYS STIF4 beam elements are then connected to this centerline node to model the axial and bending stiffness of the vent and header. Spring (STIF14) elements are used to model the vertical header supports inside the torus. ANSYS STIF4 beam elements are also used to model the stiffeners in the cylindrical region of the upper drywell. The section properties of these stiffeners are summarized in Table 3-2.

The mesh size in the sandbed region of the model was refined for the purpose of buckling evaluation. The mesh refinement was conducted as follows. Buckling analyses of flat plate finite element models with different mesh sizes were conducted and the calculated load factors were compared with the available theoretical values. The analyses considered both the fixed and free edge boundary conditions. The results of these analyses showed that with a 3"x3" mesh, the finite element predicted load factors were within a few percent of the theoretical values. Figure 3-5 shows the results of one of the flat plate analyses. Based on these analyses, it was concluded that an appropriate mesh size is achieved when the element size in the sandbed region is ≈ 3"x3". Figure 3-6 shows the view of the refined mesh. As discussed in Subsection 3.6, the refined mesh was important for the buckling analysis but had little effect on the stress magnitudes in the sandbed region.

## 3.3 Drywell Materials

The drywell shell is fabricated from SA-212, Grade B high tensile strength carbon-silicon steel plates for boilers and other pressure vessels ordered to SA-300 specifications. The mechanical properties for this material at room temperature are shown in Table 3-3. These are the properties used in the finite element analysis. For the perforated vent jet deflector, the material properties were modified to account for the reduction in stiffness due to the perforations.

## 3.4 Boundary Conditions

There are two sets of boundary conditions, one for the stress analysis and the other for the buckling analysis. The stress analysis boundary conditions are discussed first.

### 3.4.1 Boundary Conditions for Stress Analysis

Symmetric boundary conditions are defined for both edges of the 36° drywell model for the static stress analysis as shown in Figure 3-7. This allows the nodes at this boundary to expand radially outward from the drywell centerline and vertically, but not in the circumferential direction. Rotations are also fixed in two directions to prevent the boundary from rotating out of the plane of symmetry. Nodes at the bottom edge of the drywell are fixed in all directions to simulate the fixity of the shell within the concrete foundation. Nodes at the end of the header support spring elements are also fixed.

### 3.4.2 Boundary Conditions for Buckling Analysis

Three sets of boundary conditions are used at the edges of the pie slice model: symmetric at the both edges (sym-sym), symmetric at one edge and asymmetric at the other edge (sym-asym), and asymmetric at the both edges (asym-asym). This is required to capture all possible buckling mode shapes that the model is able to predict. Figure 3-8 graphically illustrates the various boundary conditions. With the symmetric boundary conditions, the nodes at the edges can displace radially but the rotation is not allowed. In the asymmetric boundary conditions, the nodes at the edges are allowed to rotate but the radial displacement is not allowed. The load factors were determined for each of the three sets of boundary conditions and the one with the smallest value was used for the Code margin evaluation.

## 3.5 Loads

The loads are applied to the drywell finite element model in the manner which most accurately represents the actual loads anticipated

on the drywell. Details on the application of loads are discussed in the following paragraphs.

3.5.1 Load Combinations

All load combinations to be considered on the drywell are summarized on Table 3-4. The most limiting load combinations in terms of possible buckling are those which cause the most compressive stresses in the sandbed region. Many of the design basis load combinations include high internal pressures which would create tensile stresses in the shell and help prevent buckling. The most severe design load combination identified for the buckling analysis of the drywell is the refueling condition (Case IV). This load combination consists of the following loads:

Dead weight of vessel, penetrations, compressible material, equipment supports and welding pads.
Live loads of welding pads and equipment door
Weight of refueling water
External Pressure of 2 psig
Seismic inertia and deflection loads for unflooded condition

The normal operation condition with seismic is very similar to this condition, however, it will be less severe due to the absence of the refueling water and equipment door weight.
The most severe load combination for the emergency condition is for the post-accident (Case VI) load combination including:

Dead weight of vessel, penetrations, compressible material and equipment supports
Live load of personnel lock
Hydrostatic Pressure of Water for Drywell Flooded to 74'-6"
External Pressure of 2 psig
Seismic inertia and deflection loads for flooded condition

The application of these loads is described in more detail in the following sections.

### 3.5.2 Gravity Loads

The gravity loads include dead weight loads of the drywell shell, weight of the compressible material and penetrations and live loads. The drywell shell loads are imposed on the model by defining the weight density of the shell material and applying a vertical acceleration of 1.0 g to simulate gravity. The ANSYS program automatically distributes the loads consistent with the mass and acceleration. The compressible material weight of 10 $lb/ft^2$ is added by adjusting the weight density of the shell to also include the compressible material. The adjusted weight densities for the various shell thicknesses are summarized in Table 3-5. The compressible material is assumed to cover the entire drywell shell (not including the vent) up to the elevation of the flange.

The additional dead weights, penetration weights and live loads are applied as additional nodal masses to the model. As shown on Table 3-6 for the refueling case, the total additional mass is summed for each 5 foot elevation of the drywell. The total is then divided by 10 for the 36° section assuming that the mass is evenly distributed around the perimeter of the drywell. The resulting mass is then applied uniformly to a set of nodes at the desired elevation as shown on Table 3-6. These applied masses automatically impose gravity loads on the drywell model with the defined acceleration of 1g. The same method is used to apply the additional masses to the model for the post-accident case as summarized in Table 3-7.

### 3.5.3 Pressure Loads

The 2 psi external pressure load for the refueling case is applied to the external faces of all of the drywell and vent shell elements. The compressive axial stress at the transition from vent shell to beam elements is simulated by applying equivalent axial forces to the nodes of the shell elements.

Considering the post-accident case, the drywell is assumed to be flooded to elevation 74'-6" (894 inches). Using a water density of

62.3 lb/ft$^3$ (0.0361 lb/in$^3$), the pressure gradient versus elevation is calculated as shown in Table 3-8. The hydrostatic pressure at the bottom of the sandbed region is calculated to be 28.3 psi. According to the elevation of the element centerline, the appropriate pressures are applied to the inside surface of the shell elements.

### 3.5.4 Seismic Loads

Seismic stresses have been calculated for the Oyster Creek Drywell in Part 1 of this report, Reference 3-3. Meridional stresses are imposed on the drywell during a seismic event due to a 0.058" deflection of the reactor building and due to horizontal and vertical inertial loads on the drywell.

The meridional stresses due to a seismic event are imposed on the 3-D drywell model by applying downward forces at four elevations of the model (A: 23'-7",B: 37'-3",C: 50'-11" and D: 88'-9") as shown on Figure 3-9. Using this method, the meridional stresses calculated in Reference 3-3 are duplicated at four sections of the drywell including 1) the mid-elevation of the sandbed region, 2) 17.25° below the equator, 3) 5.75° above the equator and 4) just above the knuckle region. These four sections were chosen to most accurately represent the load distribution in the lower drywell while also providing a reasonably accurate stress distribution in the upper drywell.

To find the correct loads to match the seismic stresses, the total seismic stress (due to reactor building deflection and horizontal and vertical inertia) are obtained from Reference 3-3 at the four sections of interest. The four sections and the corresponding meridional stresses for the refueling and post-accident seismic cases are summarized in Table 3-9.

Unit loads are then applied to the 3-D model in separate load steps at each elevation shown in Figure 3-9. The resulting stresses at the four sections of interest are then averaged for each of the applied unit loads. By solving four equations with four unknowns, the correct

loads are determined to match the stresses shown in Table 3-9 at the four sections. The calculation for the correct loads are shown on Tables 3-10 and 3-11 for the refueling and post-accident cases, respectively.

## 3.6 Stress Results

The resulting stresses for the two load combinations described in section 3.5 are summarized in this section. The mesh refinement produced less than 1% change in the calculated stress magnitudes from those obtained with the previous mesh in which the elements in the sandbed region were approx. 12"x12". The stresses reported in these Subsections are based on the refined mesh model.

### 3.6.1 Refueling Condition Stress Results

The resulting stress distributions for the refueling condition are shown in Figures 3-10 through 3-13. The red colors represent the most tensile stresses and the blue colors, the most compressive. Figures 3-10 and 3-11 show the meridional stresses for the entire drywell and lower drywell. The circumferential stresses for the same areas are shown on Figures 3-12 and 3-13. The resulting average meridional stress at the mid-elevation of the sandbed region was found to be;

$$\sigma_{Rm} = -7588 \text{ psi}$$

The circumferential stress averaged from the bottom to the top of the sandbed region is;

$$\sigma_{Rc} = 4510 \text{ psi}$$

### 3.6.2 Post-Accident Condition Stress Results

The application of all of the loads described for the post-accident condition results in the stress distributions shown in Figures 3-14 through 3-17. The red colors represent the most tensile stresses and the blue colors, the most compressive. Figures 3-14 and 3-15 show the

meridional stresses for the entire drywell and lower drywell. The circumferential stresses for the same areas are shown on Figures 3-16 and 3-17. The resulting average meridional stress at mid-elevation of the sandbed region was found to be;

$$\sigma_{PAm} = -12000 \text{ psi}$$

The circumferential stress averaged from the bottom to the top of the sandbed region is;

$$\sigma_{PAc} = +20210 \text{ psi}$$

## 3.7 Theoretical Elastic Buckling Stress Results

After the completion of stress runs for the Refueling and Post-Accident load combinations, the eigenvalue buckling runs are made as described in Section 3.1. This analysis determines the theoretical elastic buckling loads and buckling mode shapes.

### 3.7.1 Refueling Condition Buckling Results

The first buckling analysis was conducted using the sym-sym boundary conditions. The lowest (i.e., first) load factor for this case was found to be 6.14 with the critical buckling occurring in the sandbed region. The critical buckling mode shape is shown in Figure 3-18. The red color indicates sections of the shell which displace radially outward and the blue, those areas which displace inward.

The first six buckling modes were computed in this eigenvalue buckling analysis with no buckling modes found outside the sandbed region for a load factor as high as 8.89. Therefore, buckling is not a concern outside of the sandbed region.

The lowest load factors for the sym-asym and asym-asym boundary conditions were determined to be 6.23 and 7.22, respectively. Figure 3-19 shows the buckling mode shape with sym-asym boundary conditions. It is clear from these load factor values that the sym-sym boundary

condition load factor of 6.14 is the lowest one. Multiplying the load factor of 6.14 by the average meridional stress from section 3.6.1, the theoretical elastic buckling stress is found to be;

$$\sigma_{Rie} = 6.14 \times (7588 \text{ psi}) = 46590 \text{ psi}$$

3.7.2 Post-Accident Condition Buckling Results

Considering the post-accident case with symmetric boundary conditions, the load factor was calculated as 4.085. The sym-asym boundary conditions gave a load factor of 4.206 for the first mode. Based on the refueling condition buckling analyses, it was concluded that the load factor for the asym-asym condition will be higher than both the sym-sym and sym-asym load factors. Thus, the sym-sym boundary conditions gave the lowest load factor and thus are controlling. The critical mode shape for the sym-sym boundary conditions is shown in Figure 3-20. As expected, this mode shape is associated with the sandbed region.

Multiplying the load factor of 4.085 by the applied stress from section 3.6.2 results in a theoretical elastic buckling stress of

$$\sigma_{PAie} = 4.085 \times (12000 \text{ psi}) = 49020 \text{ psi}$$

3.8 References

3-1 DeSalvo, G.J., Ph.D, and Gorman, R.W., "ANSYS Engineering Analysis System User's Manual, Revision 4.4," Swanson Analysis Systems, Inc., May 1, 1989.

3-2 GPUN Specification SP-1302-53-044, Technical Specification for Primary Containment Analysis - Oyster Creek Nuclear Generating Station; Rev. 2, October 1990.

3-3 "An ASME Section VIII Evaluation of the Oyster Creek Drywell - Part 1 Stress Analysis," GE Report No. 9-1, DRF # 00664, November 1990, prepared for GPUN.

Table 3-1

Oyster Creek Drywell Shell Thicknesses

| Section | Thickness (in.) |
|---|---|
| Sandbed Region | 0.736 * |
| Lower Sphere | 1.154 |
| Mid Sphere | 0.770 |
| Upper Sphere | 0.722 |
| Knuckle | 2.5625 |
| Cylinder | 0.640 |
| Reinforcement Below Flange | 1.250 |
| Reinforcement Above Flange | 1.500 |
| Elliptical Head | 1.1875 |
| Ventline Reinforcement | 2.875 |
| Gussets | 0.875 |
| Vent Jet Deflector | 2.500 |
| Ventline Connection | 2.500 |
| Upper Ventline | 0.4375 |
| Lower Ventline | 0.250 |

* 95% confidence projected thickness to 14R.

Table 3-2

Cylinder Stiffener Locations and Section Properties

| Elevation (in) | Height (in) | Width (in) | Area ($in^2$) | Bending Inertia ($in^4$) Horizontal | Vertical |
|---|---|---|---|---|---|
| 966.3 | 0.75 | 6.0 | 4.5 | 13.5 | 0.211 |
| 1019.8 | 0.75 | 6.0 | 4.5 | 13.5 | 0.211 |
| 1064.5 | 0.50 | 6.0 | 3.0 | 9.0 | 0.063 |
| 1113.0(1) | 2.75<br>1.00 | 7.0<br>7.38 | 26.6 | 387.5 | 12.75 |
| 1131.0 | 1.0 | 12.0 | 12.0 | 144.0 | 1.000 |

(1) - This stiffener is made up of 2 beam sections, one 2.75x7" and one 1.0x7.375"

Table 3-3

Material Properties for SA-212 Grade B Steel

| Material Property | Value |
|---|---|
| Young's Modulus | $29.6 \times 10^6$ psi |
| Yield Strength | 38000 psi |
| Poisson's Ratio | 0.3 |
| Density | 0.283 $lb/in^3$ |

Table 3-4

Oyster Creek Drywell Load Combinations

CASE I - INITIAL TEST CONDITION
Deadweight + Design Pressure (62 psi) + Seismic (2 x DBE)

CASE II - FINAL TEST CONDITION
Deadweight + Design Pressure (35 psi) + Seismic (2 x DBE)

CASE III - NORMAL OPERATING CONDITION
Deadweight + Pressure (2 psi external) + Seismic (2 x DBE)

CASE IV - REFUELING CONDITION
Deadweight + Pressure (2 psi external) + Water Load +
Seismic (2 x DBE)

CASE V - ACCIDENT CONDITION
Deadweight + Pressure(62 psi @ 175°F or 35 psi @ 281°F) +
Seismic (2 x DBE)

CASE VI - POST ACCIDENT CONDITION
Deadweight + Water Load @ 74'6" + Seismic (2 x DBE)

Table 3-5

Adjusted Weight Densities of Shell to Account for Compressible Material Weight

| Shell Thickness (in.) | Adjusted Weight Density ($lb/in^3$) |
|---|---|
| 1.154 | 0.343 |
| 0.770 | 0.373 |
| 0.722 | 0.379 |
| 2.563 | 0.310 |
| 0.640 | 0.392 |
| 1.250 | 0.339 |

Table 3-6

Oyster Creek Drywell Additional Weights - Refueling Condition

| ELEVATION (feet) | DEAD WEIGHT (lbf) | PENETR. WEIGHT (lbf) | & MISC. LOADS (lbf) | TOTAL LOAD (lbf) | 5 FOOT RANGE LOAD | LOAD PER 36 DEG. (lbf) | # OF ELEMENTS | NODES OF APPLICATION | LOAD PER FULL NODE (lbf) | LOAD PER HALF NODE (lbf) |
|---|---|---|---|---|---|---|---|---|---|---|
| 15.56 | 50000 | | | 50000 | | | | | | |
| 16 | | 168100 | | 168100 | | | | | | |
| 20 | | 11200 | | 11200 | | | | | | |
| ** 15-20 | | | | | 229300 | 22930 | 8 | 116-119 | 3822 | 1911 |
| 22# | 556000 | | | 556000 | | | | | | |
| ** 21-25# | | | | | 556000 | 55600 | 8 | 161-169 | 6950 | 3475 |
| 26 | | 11100 | | 11100 | | | | | | |
| 30 | 64100 | 51500 | | 115600 | | | | | | |
| 30.25 | 105000 | | 100000 | 205000 | | | | | | |
| ** 26-30 | | | | | 331700 | 33170 | 8 | 179-187 | 4146 | 2073 |
| 31 | | 16500 | | 16500 | | | | | | |
| 32 | | 750 | | 750 | | | | | | |
| 33 | | 15450 | | 15450 | | | | | | |
| 34 | | 28050 | | 28050 | | | | | | |
| 35 | | 1500 | | 1500 | | | | | | |
| ** 31-35 | | | | | 62250 | 6225 | 8 | 188-196 | 778 | 389 |
| 36 | | 1550 | | 1550 | | | | | | |
| 40 | 41000 | 43350 | | 84350 | | | | | | |
| ** 36-40 | | | | | 85900 | 8590 | 8 | 197-205 | 1074 | 537 |
| 50# | 1102000 | | | 1102000 | | | | | | |
| ** 45-50# | | | | | 1102000 | 110200 | 8 | 418-426 | 13775 | 6888 |
| 54 | | 7850 | | 7850 | | | | | | |
| ** 51-55 | | | | | 7850 | 785 | 8 | 436-444 | 98 | 49 |
| 56 | 56400 | | 24000 | 80400 | | | | | | |
| 60 | 95200 | 700 | 20000 | 115900 | | | | | | |
| ** 56-60 | | | | | 196300 | 19630 | 8 | 454-462 | 2454 | 1227 |
| 65 | 52000 | | 20000 | 72000 | | | | | | |
| ** 61-65 | | | | | 72000 | 7200 | 8 | 472-480 | 900 | 450 |
| 70 | | 5750 | | 5750 | | | | | | |
| ** 66-70 | | | | | 5750 | 575 | 8 | 508-516 | 72 | 36 |
| 73 | | 8850 | | 8850 | | | | | | |
| ** 71-75 | | | | | 8850 | 885 | 8 | 526-534 | 111 | 55 |
| 82.17 | 21650 | | | 21650 | | | | | | |
| ** 81-85 | | | | | 21650 | 2165 | 8 | 553-561 | 271 | 135 |
| 87 | | 1000 | | 1000 | | | | | | |
| 90 | | 15000 | | 15000 | | | | | | |
| ** 86-90 | | | | | 16000 | 1600 | 8 | 571-579 | 200 | 100 |
| 93.75 | 20700 | | | 20700 | | | | | | |
| 94.75# | | | 698000 | 698000 | | | | | | |
| 95.75 | 20100 | | | 20100 | | | | | | |
| ** 91-96 | | | | | 738800 | 73880 | 8 | 589-597 | 9235 | 4618 |
| TOTALS: | 2184150 | 388200 | 862000 | 3434350 | 3434350 | 343435 | | | | |

\# - LOAD TO BE APPLIED IN VERTICAL DIRECTION ONLY.

& - MISCELLANEOUS LOADS INCLUDE 698000 LB WATER WEIGHT AT 94.75 FT. ELEVATION 100000 LB EQUIPMENT DOOR WEIGHT AT 30.25 FT. ELEVATION AND WELD PAD LIVE LOADS OF 24000, 20000 AND 20000 AT 56, 60 AND 65 FT. ELEVATIONS

REFWGT.WK1

## Table 3-7

## Oyster Creek Drywell Additional Weights - Post-Accident Condition

| ELEVATION (feet) | DEAD WEIGHT (lbf) | PENETR. WEIGHT (lbf) | & MISC. LOADS (lbf) | TOTAL LOAD (lbf) | 5 FOOT RANGE LOAD | LOAD PER 36 DEG. (lbf) | # OF ELEMENTS | NODES OF APPLICATION | LOAD PER FULL NODE (lbf) | LOAD PER HALF NODE (lbf) |
|---|---|---|---|---|---|---|---|---|---|---|
| 15.56 | 50000 | | | 50000 | | | | | | |
| 16 | | 168100 | | 168100 | | | | | | |
| 20 | | 11200 | | 11200 | | | | | | |
| ** 15-20 | | | | | 229300 | 22930 | 6 | 116-119 | 3822 | 1911 |
| 22# | 556000 | | | 556000 | | | | | | |
| ** 21-25# | | | | | 556000 | 55600 | 8 | 161-169 | 6950 | 3475 |
| 26 | | 11100 | | 11100 | | | | | | |
| 30 | 64100 | 51500 | | 115600 | | | | | | |
| 30.25 | 105000 | | | 105000 | | | | | | |
| ** 26-30 | | | | | 231700 | 23170 | 8 | 179-187 | 2896 | 1448 |
| 31 | | 16500 | | 16500 | | | | | | |
| 32 | | 750 | | 750 | | | | | | |
| 33 | | 15450 | | 15450 | | | | | | |
| 34 | | 28050 | | 28050 | | | | | | |
| 35 | | 1500 | | 1500 | | | | | | |
| ** 31-35 | | | | | 62250 | 6225 | 8 | 188-196 | 778 | 389 |
| 36 | | 1550 | | 1550 | | | | | | |
| 40 | 41000 | 43350 | | 84350 | | | | | | |
| ** 36-40 | | | | | 85900 | 8590 | 8 | 197-205 | 1074 | 537 |
| 50# | 1102000 | | | 1102000 | | | | | | |
| ** 45-50# | | | | | 1102000 | 110200 | 8 | 418-426 | 13775 | 6888 |
| 54 | | 7850 | | 7850 | | | | | | |
| ** 51-55 | | | | | 7850 | 785 | 8 | 436-444 | 98 | 49 |
| 56 | 56400 | | | 56400 | | | | | | |
| 60 | 95200 | 700 | | 95900 | | | | | | |
| ** 56-60 | | | | | 152300 | 15230 | 8 | 454-462 | 1904 | 952 |
| 65 | 52000 | | | 52000 | | | | | | |
| ** 61-65 | | | | | 52000 | 5200 | 8 | 472-480 | 650 | 325 |
| 70 | | 5750 | | 5750 | | | | | | |
| ** 66-70 | | | | | 5750 | 575 | 8 | 508-516 | 72 | 36 |
| 73 | | 8850 | | 8850 | | | | | | |
| ** 71-75 | | | | | 8850 | 885 | 8 | 526-534 | 111 | 55 |
| 82.17 | 21650 | | | 21650 | | | | | | |
| ** 81-85 | | | | | 21650 | 2165 | 8 | 553-561 | 271 | 135 |
| 87 | | 1000 | | 1000 | | | | | | |
| 90 | | 15000 | | 15000 | | | | | | |
| ** 86-90 | | | | | 16000 | 1600 | 8 | 571-579 | 200 | 100 |
| 93.75 | 20700 | | | 20700 | | | | | | |
| 95.75 | 20100 | | | 20100 | | | | | | |
| ** 91-96 | | | | | 40800 | 4080 | 8 | 589-597 | 510 | 255 |
| TOTALS: | 2184150 | 388200 | 0 | 2572350 | 2572350 | 257235 | | | | |

\# - LOAD TO BE APPLIED IN VERTICAL DIRECTION ONLY.
& - NO MISCELLANEOUS LOADS FOR THIS CONDITION.

FLOODWGT.WK1

Table 3-8

Hydrostatic Pressures for Post-Accident, Flooded Condition

WATER DENSITY: 62.32 lb/ft3
0.03606 lb/in3

FLOODED ELEV: 74.5 ft
894 inches

| ELEMENTS ABOVE NODES | ANGLE ABOVE EQUATOR (degrees) | ELEVATION (inch) | DEPTH (inch) | PRESSURE (psi) | ELEMENTS |
|---|---|---|---|---|---|
| 27 | -53.32 | 110.2 | 783.8 | 28.3 | 1-12 |
| 40 | -51.97 | 116.2 | 777.8 | 28.1 | 13-24 |
| 53 | -50.62 | 122.4 | 771.6 | 27.8 | 25-36 |
| 66 | -49.27 | 128.8 | 765.2 | 27.6 | 37-48 |
| 79 | -47.50 | 137.3 | 756.7 | 27.3 | 49-51, 61-66 ,55-57 |
| 92 | -46.20 | 143.9 | 750.1 | 27.1 | 52-54, 138-141 ,58-60 |
| 102 | -44.35 | 153.4 | 740.6 | 26.7 | 142-147, 240-242, 257-259 |
| 108 | -41.89 | 166.6 | 727.4 | 26.2 | 148-151, 243, 256 |
| 112 | -39.43 | 180.2 | 713.8 | 25.7 | 152-155, 244, 255 |
| 116 | -36.93 | 194.6 | 699.4 | 25.2 | 156-159, 245, 254 |
| 120 | -34.40 | 209.7 | 684.3 | 24.7 | 160-165, 246, 253 |
| 124 | -31.87 | 225.2 | 668.8 | 24.1 | 166-173, 247, 252 |
| 130 | -29.33 | 241.3 | 652.7 | 23.5 | 174-183, 248-251 |
| 138 | -26.80 | 257.6 | 636.4 | 23.0 | 184-195 |
| 148 | -24.27 | 274.4 | 619.6 | 22.3 | 196-207 |
| 161 | -20.13 | 302.5 | 591.5 | 21.3 | 208-215 |
| 170 | -14.38 | 342.7 | 551.3 | 19.9 | 216-223 |
| 179 | -8.63 | 384.0 | 510.0 | 18.4 | 224-231 |
| 188 | -2.88 | 425.9 | 468.1 | 16.9 | 232-239 |
| 197 | 2.88 | 468.1 | 425.9 | 15.4 | 430-437 |
| 400 | 8.63 | 510.0 | 384.0 | 13.8 | 438-445 |
| 409 | 14.38 | 551.3 | 342.7 | 12.4 | 446-453 |
| 418 | 20.13 | 591.5 | 302.5 | 10.9 | 454-461 |
| 427 | 25.50 | 627.8 | 266.2 | 9.6 | 462-469 |
| 436 | 30.50 | 660.2 | 233.8 | 8.4 | 470-477 |
| 445 | 35.50 | 690.9 | 203.1 | 7.3 | 478-485 |
| 454 | 40.50 | 719.8 | 174.2 | 6.3 | 486-493 |
| 463 | 45.50 | 746.6 | 147.4 | 5.3 | 494-501 |
| 472 | 50.50 | 771.1 | 122.9 | 4.4 | 502-509 |
| 481 | 54.86 | 790.5 | 103.5 | 3.7 | 510-517 |
| 490 | - | 805.6 | 88.4 | 3.2 | 518-525 |
| 499 | - | 820.7 | 73.3 | 2.6 | 526-533 |
| 508 | - | 835.7 | 58.3 | 2.1 | 534-541 |
| 517 | - | 850.8 | 43.2 | 1.6 | 542-549 |
| 526 | - | 885.3 | 8.7 | 0.3 | 550-557 |
| - | - | 187.3 | 706.7 | 25.5 | 340-399 (Ventline) |

FLOODP.WK1

Table 3-9

Meridional Seismic Stresses at Four Sections

| Section | Elevation (inches) | 2-D Shell Model Node | Meridional Stresses Refueling (psi) | Meridional Stresses Post-Accident (psi) |
|---|---|---|---|---|
| A) Middle of Sandbed | 119 | 32 | 1258 | 1288 |
| B) 17.25° Below Equator | 323 | 302 | 295 | 585 |
| C) 5.75° Above Equator | 489 | 461 | 214 | 616 |
| D) Above Knuckle | 1037 | 1037 | 216 | 808 |

# Table 3-10

## Application of Loads to Match Seismic Stresses - Refueling Case

| COMPRESSIVE STRESSES FROM 2-D ANALYSIS | SECTION: | 2-D SEISMIC STRESSES AT SECTION (psi) 1 | 2 | 3 | 4 |
|---|---|---|---|---|---|
| | 2-D NODE: | 32 | 302 | 461 | 1037 |
| | ELEV: | 119.3" | 322.5" | 489.1" | 912.3" |
| 0.058" SEISMIC DEFLECTION: | | 788.67 | 155.54 | 103.46 | 85.31 |
| HORIZ. PLUS VERTICAL SEISMIC INERTIA: | | 469.55 | 139.44 | 110.13 | 130.21 |
| TOTAL SEISMIC COMPRESSIVE STRESSES: | | 1258.22 | 294.98 | 213.59 | 215.52 |

| 3-D INPUT LOAD SECTION | INPUT 3-D UNIT LOAD DESCRIPTION | SECTION: | 3-D STRESSES AT SECTION (psi) 1 | 2 | 3 | 4 |
|---|---|---|---|---|---|---|
| | | 3-D NODES: | 53-85 | 170-178 | 400-408 | 526-534 |
| | | ELEV: | 119.3" | 322.5" | 489.1" | 912.3" |
| A | 1000 lbs at nodes 563 through 569 | | 85.43 | 37.04 | 34.94 | 55.23 |
| B | 500 lbs at 427&435, 1000 lbs at 428-434 | | 89.88 | 39.92 | 36.76 | 0.00 |
| C | 500 lbs at 197&205, 1000 lbs at 198-204 | | 97.64 | 43.37 | 0.00 | 0.00 |
| D | 500 lbs at 161&169, 1000 lbs at 162-168 | | 89.85 | 0.00 | 0.00 | 0.00 |
| | DESIRED COMPRESSIVE STRESSES (psi): | | 1258.22 | 294.98 | 213.59 | 215.52 |

| 3-D INPUT LOAD SECTION | LOAD TO BE APPLIED TO MATCH 2-D STRESSES | | RESULTING STRESSES AT SECTION (psi) | | | |
|---|---|---|---|---|---|---|
| A | 3902.2 | | 333.37 | 148.05 | 136.34 | 215.52 |
| B | 2101.4 | | 188.87 | 83.89 | 77.25 | 0.00 |
| C | 1453.6 | | 141.93 | 63.04 | 0.00 | 0.00 |
| D | 6611.6 | | 594.05 | 0.00 | 0.00 | 0.00 |
| | | SUM: | 1258.22 | 294.98 | 213.59 | 215.52 |

SEISUNFL.WK1

# Table 3-11

## Application of Loads to Match Seismic Stresses - Post-Accident Case

| COMPRESSIVE STRESSES FROM 2-D ANALYSIS | 2-D SEISMIC STRESSES AT SECTION (psi) | | | |
|---|---|---|---|---|
| SECTION: | 1 | 2 | 3 | 4 |
| 2-D NODE: | 32 | 302 | 461 | 1037 |
| ELEV: | 119.3" | 322.5" | 489.1" | 912.3" |
| 0.058" SEISMIC DEFLECTION: | 788.67 | 155.54 | 103.46 | 85.31 |
| HORIZ. PLUS VERTICAL SEISMIC INERTIA: | 499.79 | 429.39 | 512.76 | 723.14 |
| TOTAL SEISMIC COMPRESSIVE STRESSES: | 1288.46 | 584.93 | 616.22 | 808.45 |

| 3-D INPUT LOAD SECTION | INPUT 3-D UNIT LOAD DESCRIPTION | 3-D STRESSES AT SECTION (psi) | | | |
|---|---|---|---|---|---|
| SECTION: | | 1 | 2 | 3 | 4 |
| 3-D NODES: | | 53-65 | 170-178 | 400-408 | 526-534 |
| ELEV: | | 119.3" | 322.5" | 489.1" | 912.3" |
| A | 1000 lbs at nodes 563 through 569 | 85.43 | 37.94 | 34.94 | 55.23 |
| B | 500 lbs at 427&435, 1000 lbs at 428-434 | 89.88 | 39.92 | 36.76 | 0.00 |
| C | 500 lbs at 197&205, 1000 lbs at 198-204 | 97.64 | 43.37 | 0.00 | 0.00 |
| D | 500 lbs at 161&169, 1000 lbs at 162-168 | 89.85 | 0.00 | 0.00 | 0.00 |
| DESIRED COMPRESSIVE STRESSES (psi): | | 1288.46 | 584.93 | 616.22 | 808.45 |

| 3-D INPUT LOAD SECTION | LOAD TO BE APPLIED TO MATCH 2-D STRESSES | RESULTING STRESSES AT SECTION (psi) | | | |
|---|---|---|---|---|---|
| A | 14837.9 | 1250.51 | 555.36 | 511.45 | 808.45 |
| B | 2850.2 | 256.17 | 113.78 | 104.77 | 0.00 |
| C | -1941.7 | -189.58 | -84.21 | 0.00 | 0.00 |
| D | -318.8 | -28.64 | 0.00 | 0.00 | 0.00 |
| SUM: | | 1288.46 | 584.93 | 616.22 | 808.45 |

SEISFL.WK1

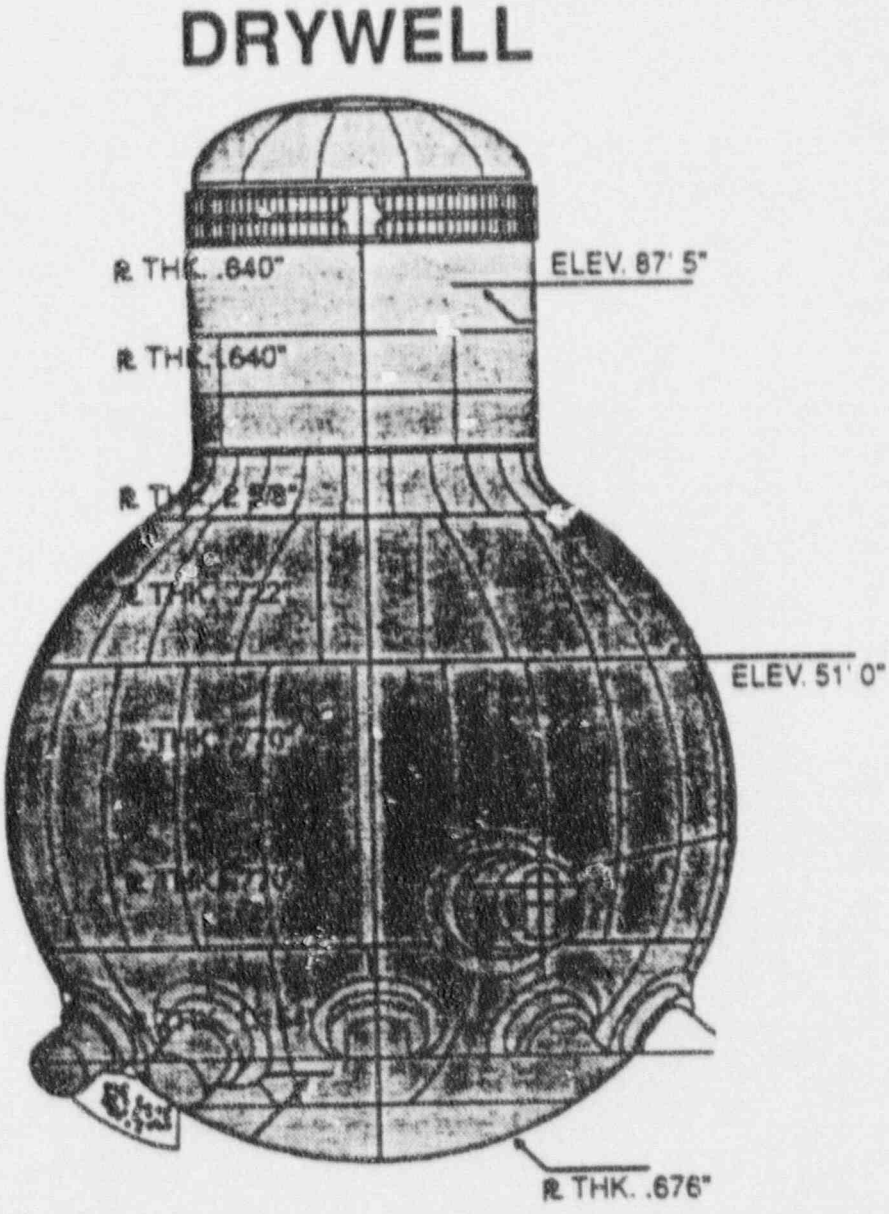


Figure 3-1. Oyster Creek Drywell Geometry

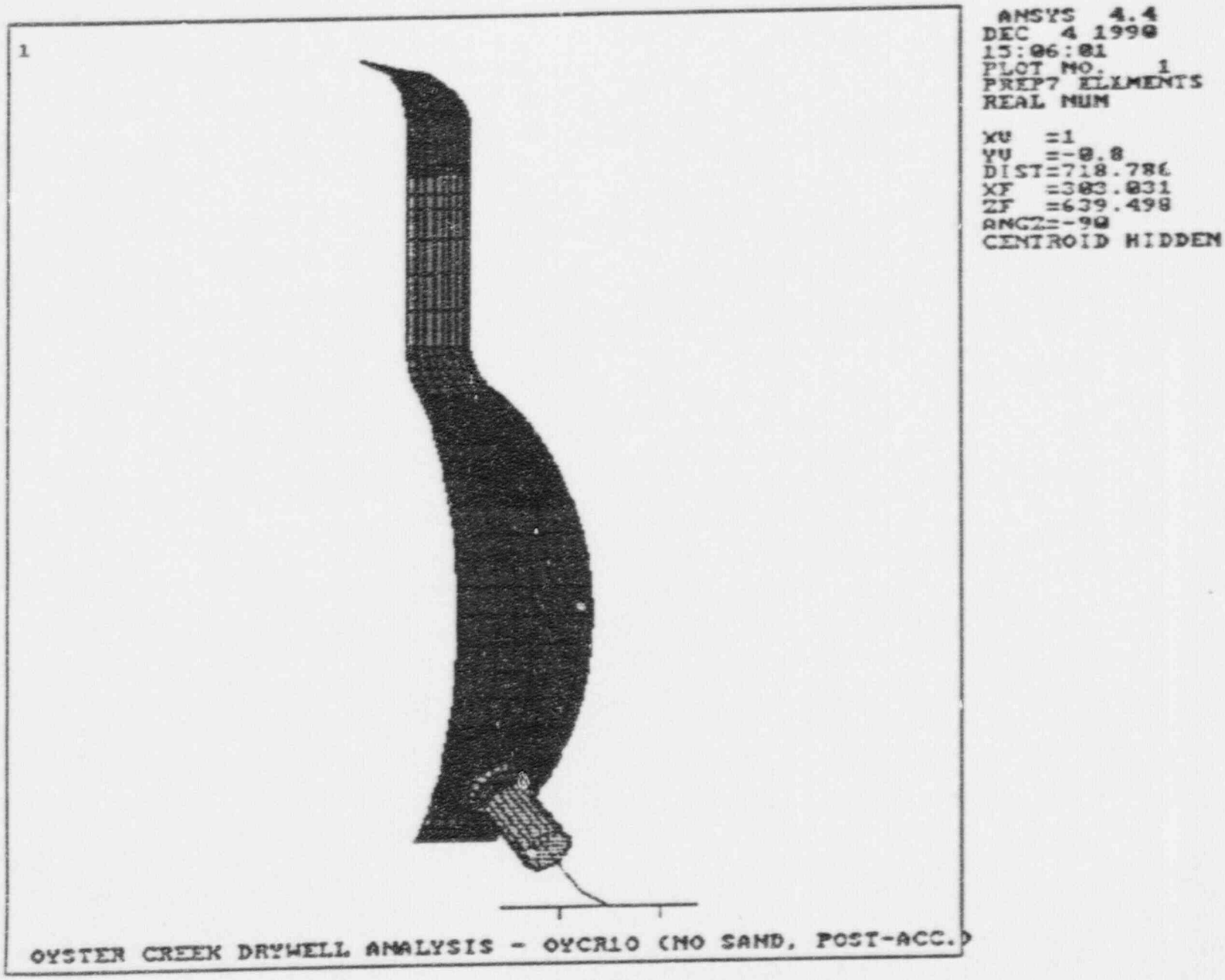


Figure 3-2. Oyster Creek Drywell 3-D Finite Element Model

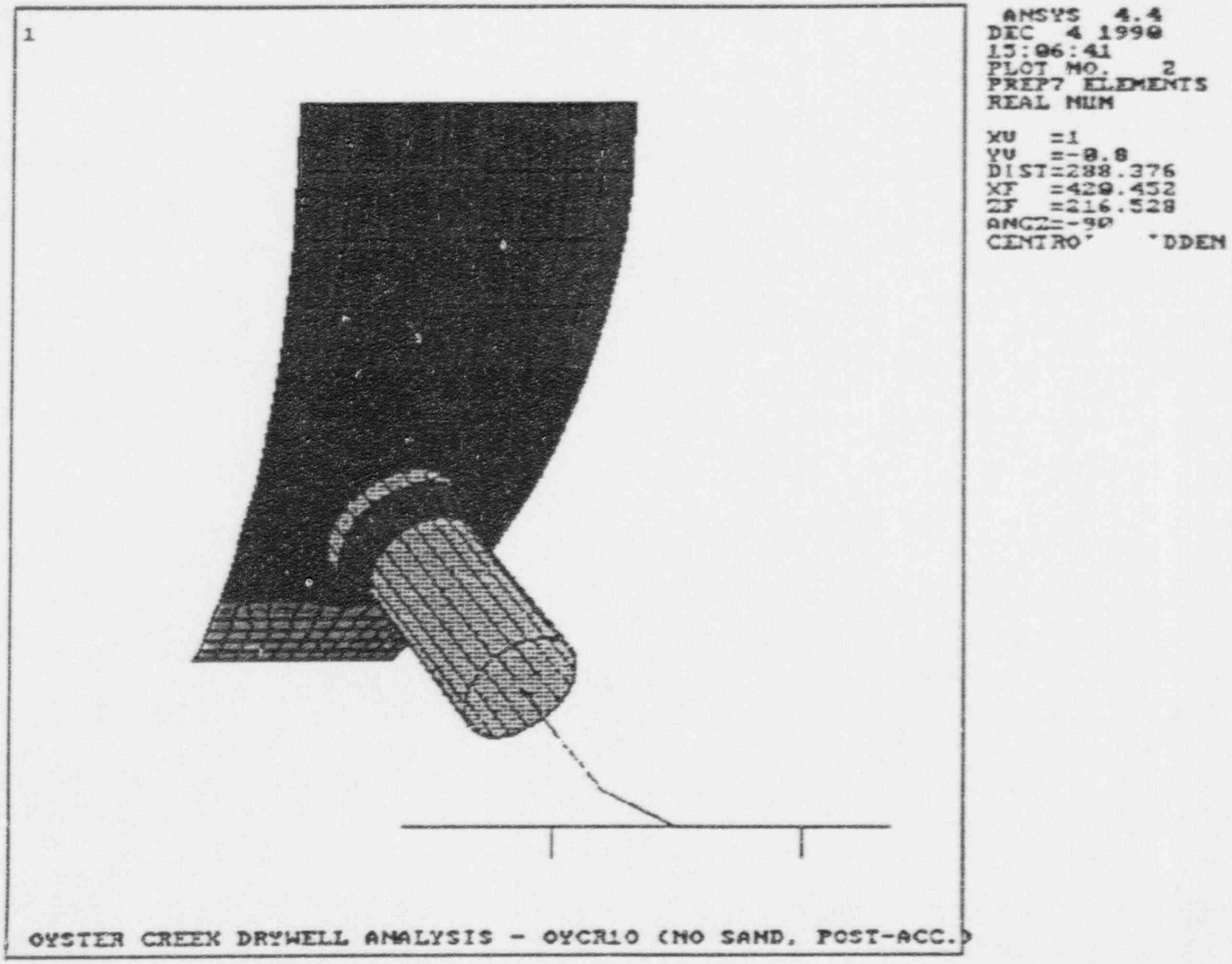


Figure 3-3. Closeup of Lower Drywell Section of FEM (Outside View)

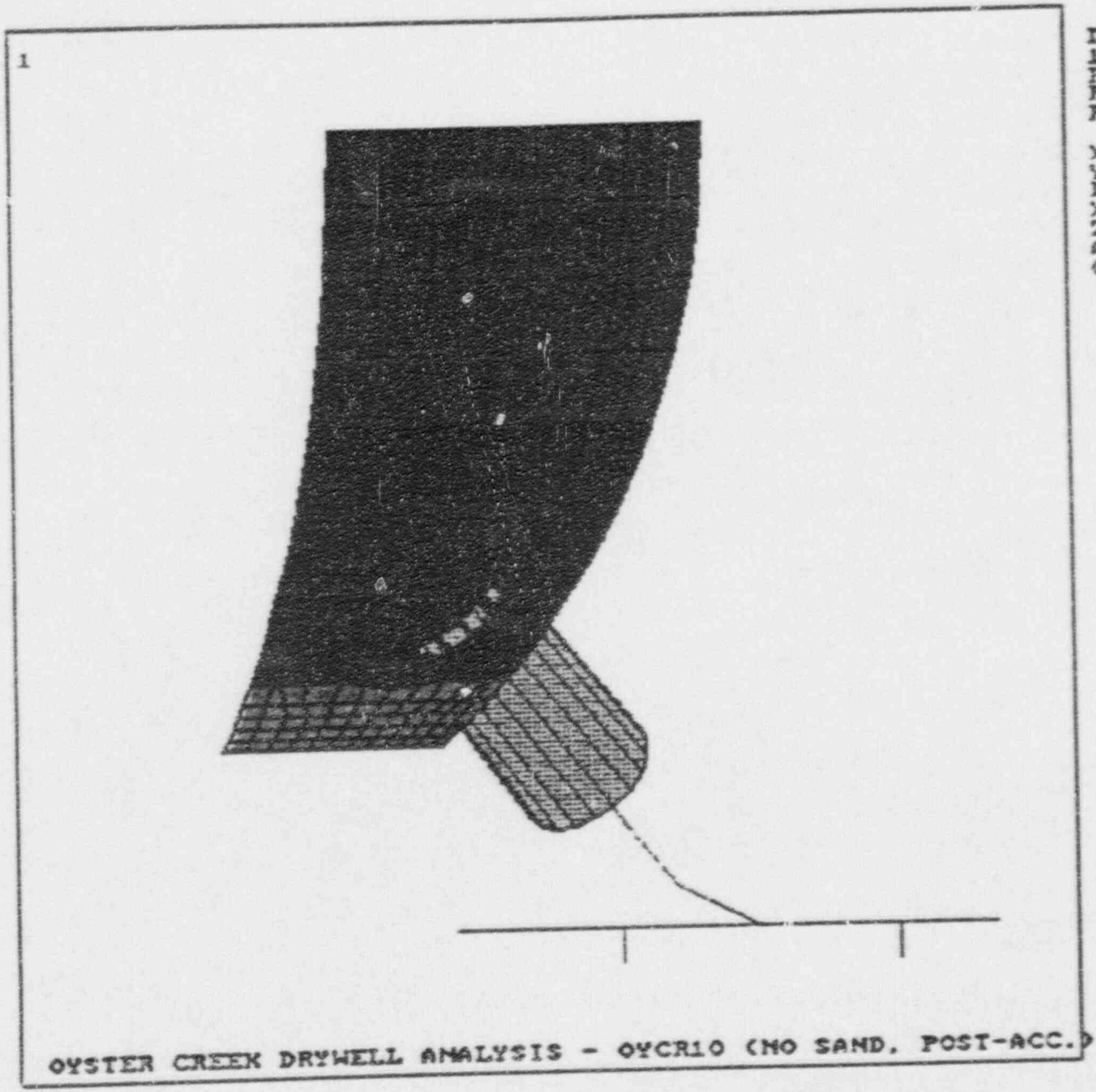


Figure 3-4. Closeup of Lower Drywell Section of FEM (Inside View)

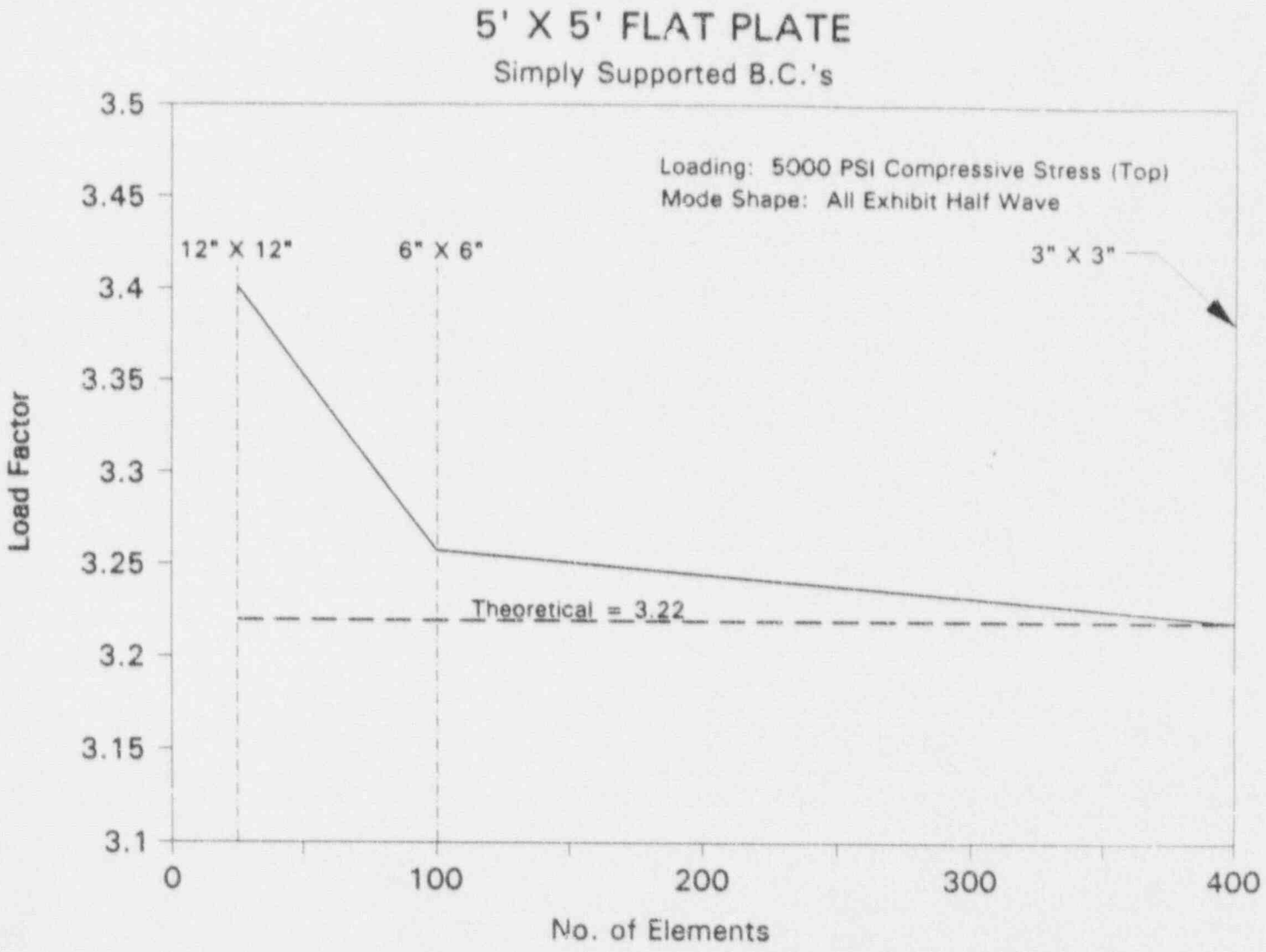


Figure 3-5. Flat Plate Buckling Analysis Results for Free Edge Boundary Conditions

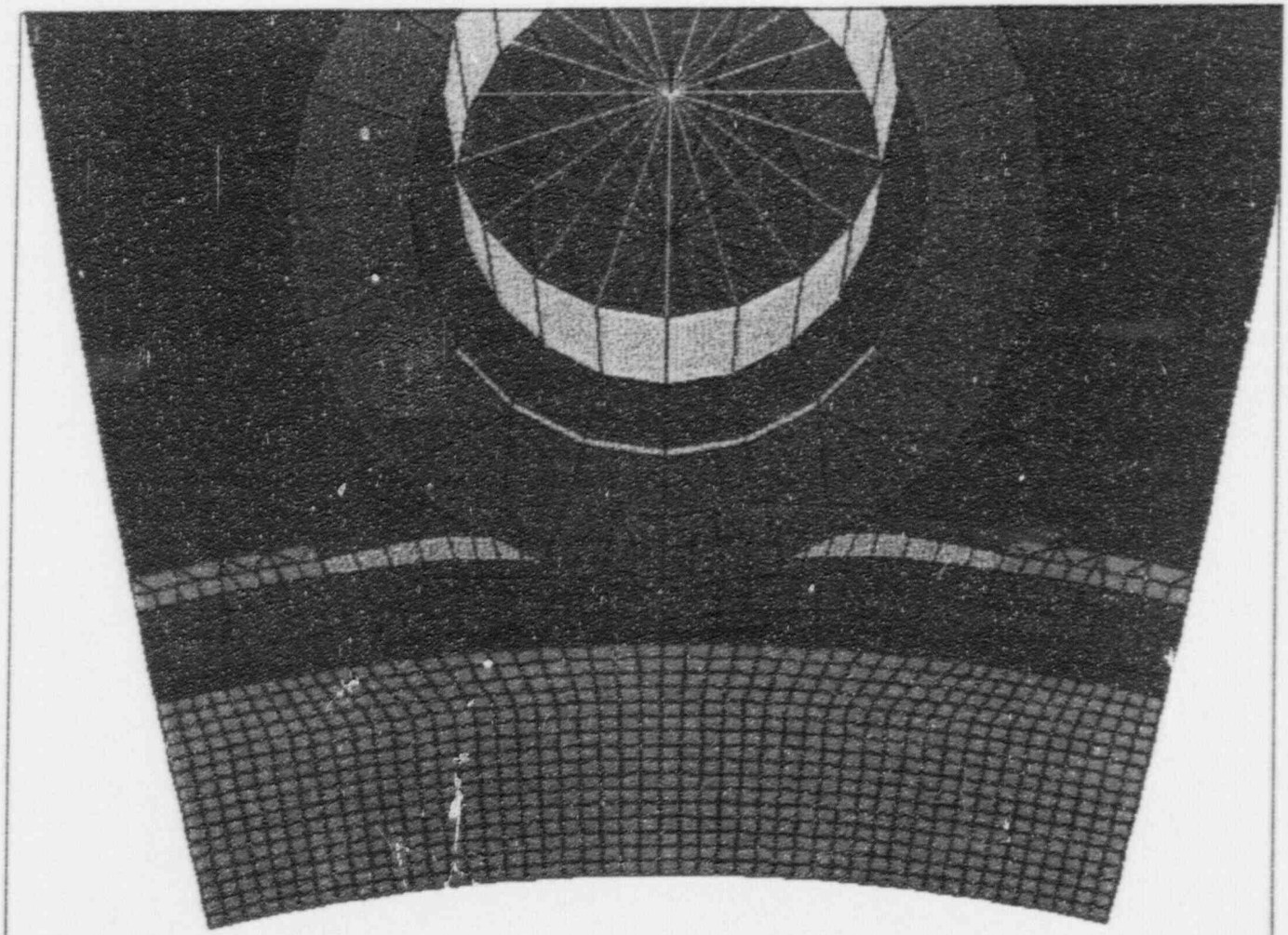


Figure 3-6 View of Refined Mesh in the Sandbed Region

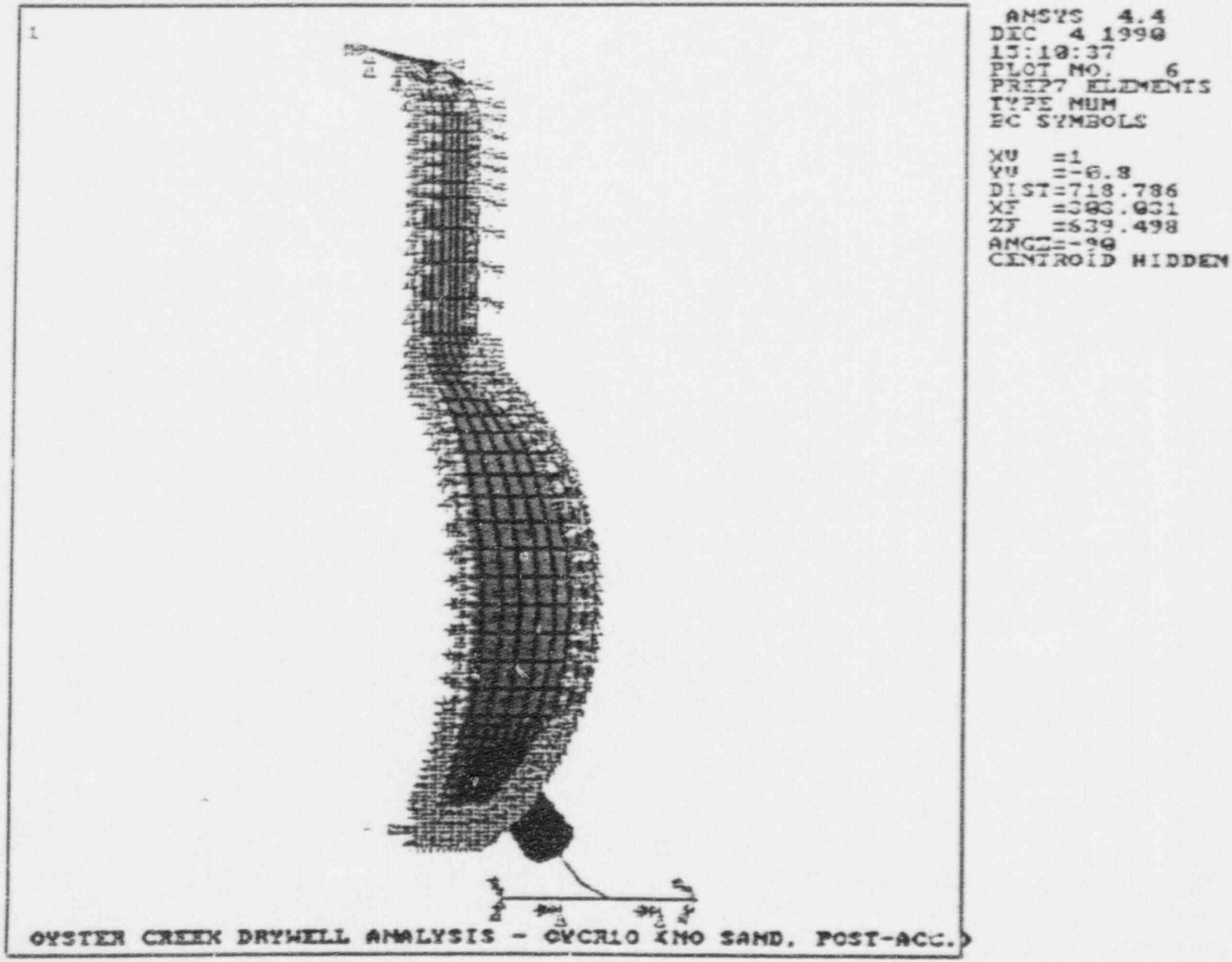


Figure 3-7 Symmetric Boundary Conditions for Stress Analysis

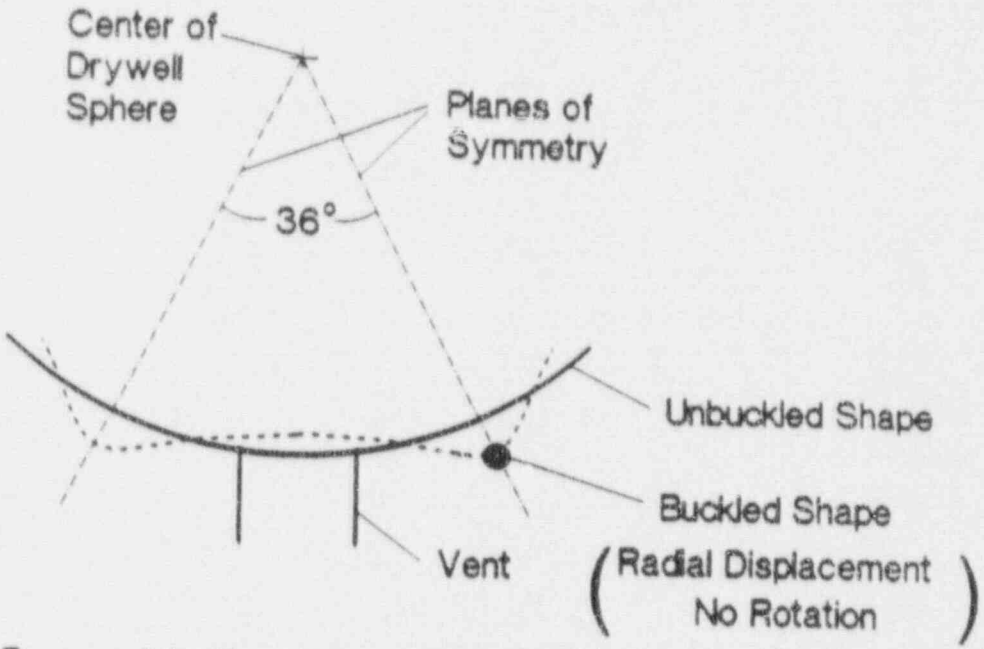


Symmetric Buckling of Drywell

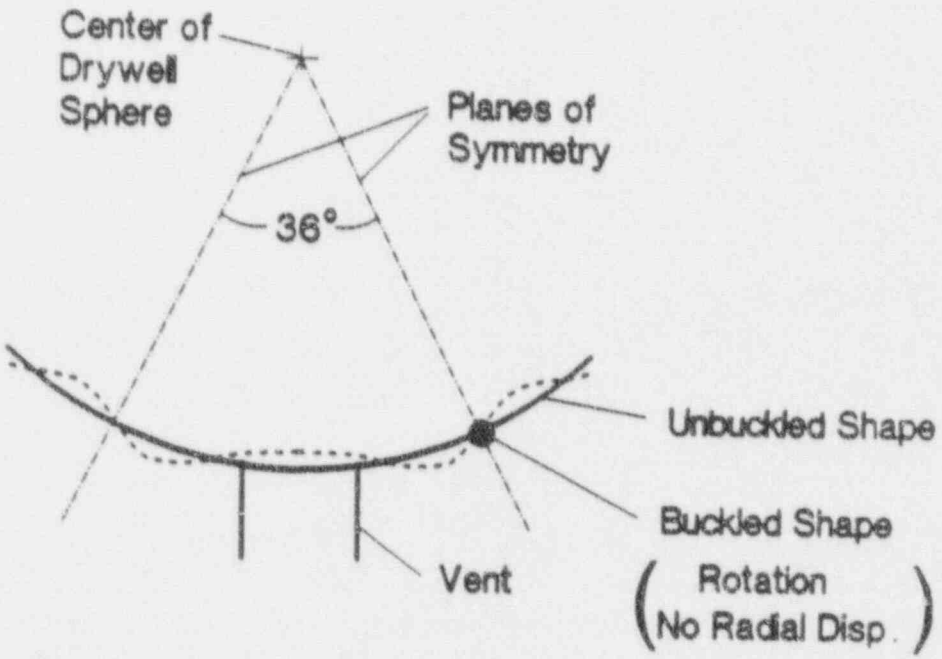


Asymmetric Buckling of Drywell

SYM.DRW

Figure 3-8 Symmetric and Asymmetric Buckling Modes

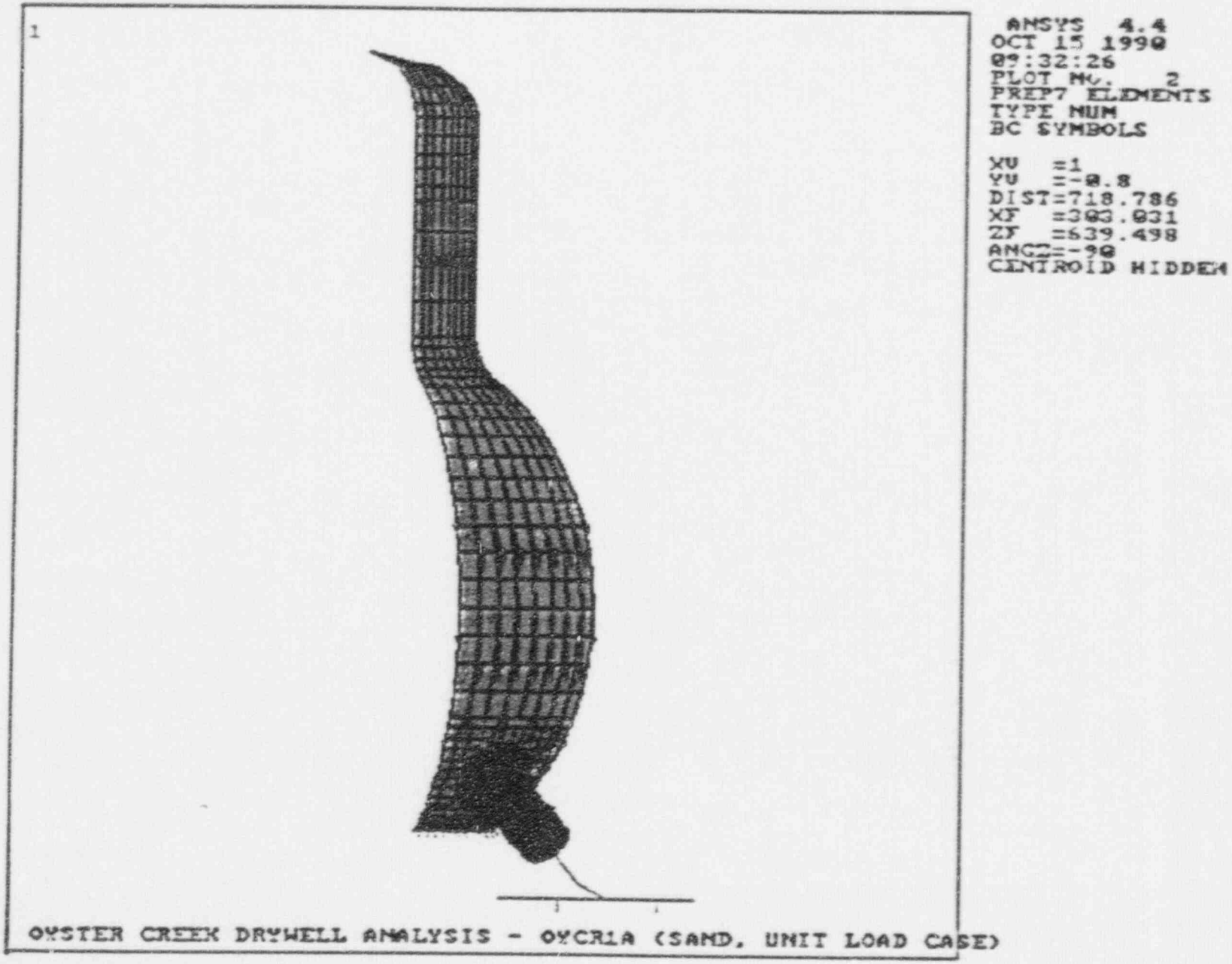


Figure 3-9 Application of Loading to Simulate Seismic Bending

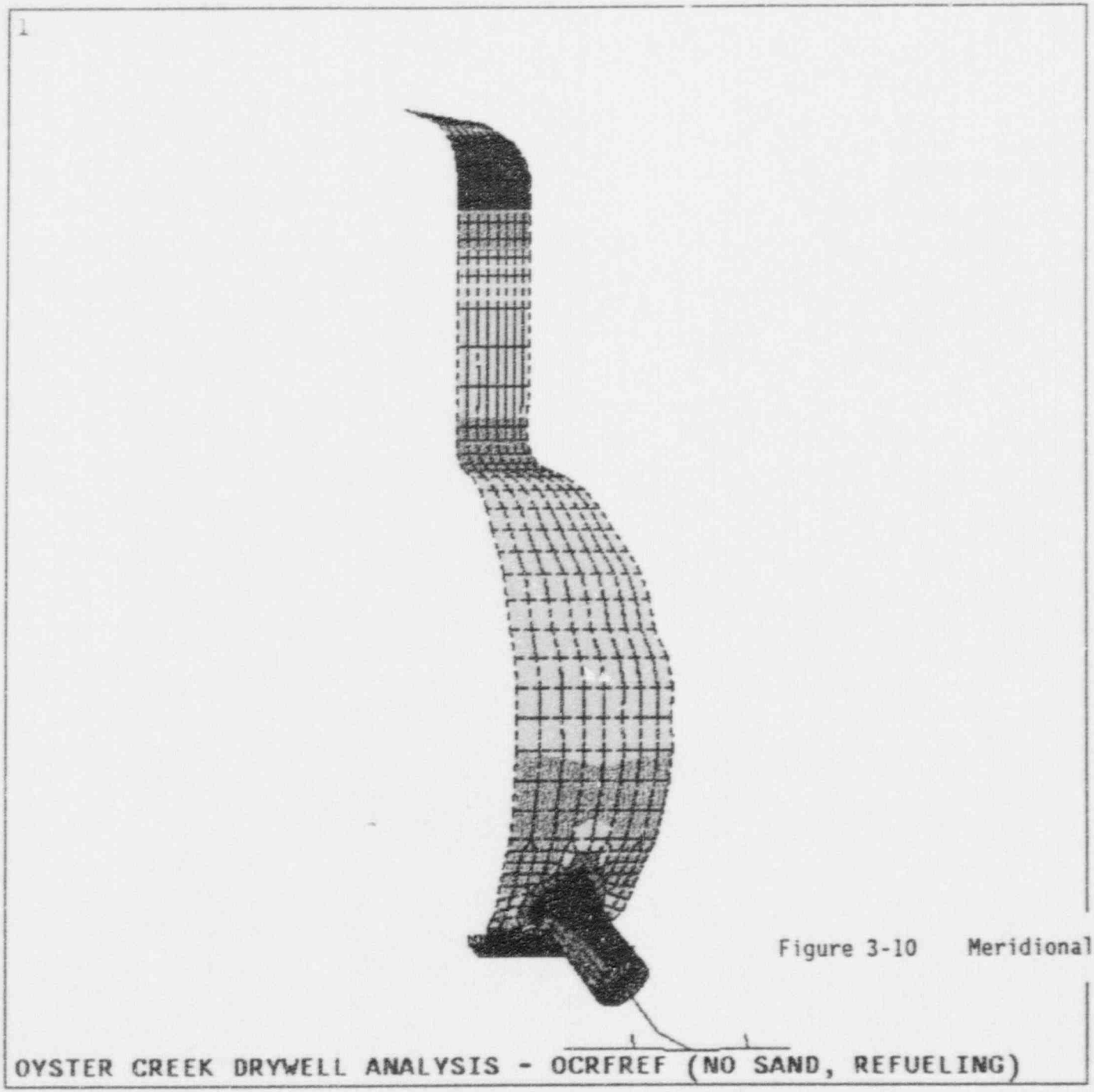


Figure 3-10 Meridional Stresses - Refueling Case

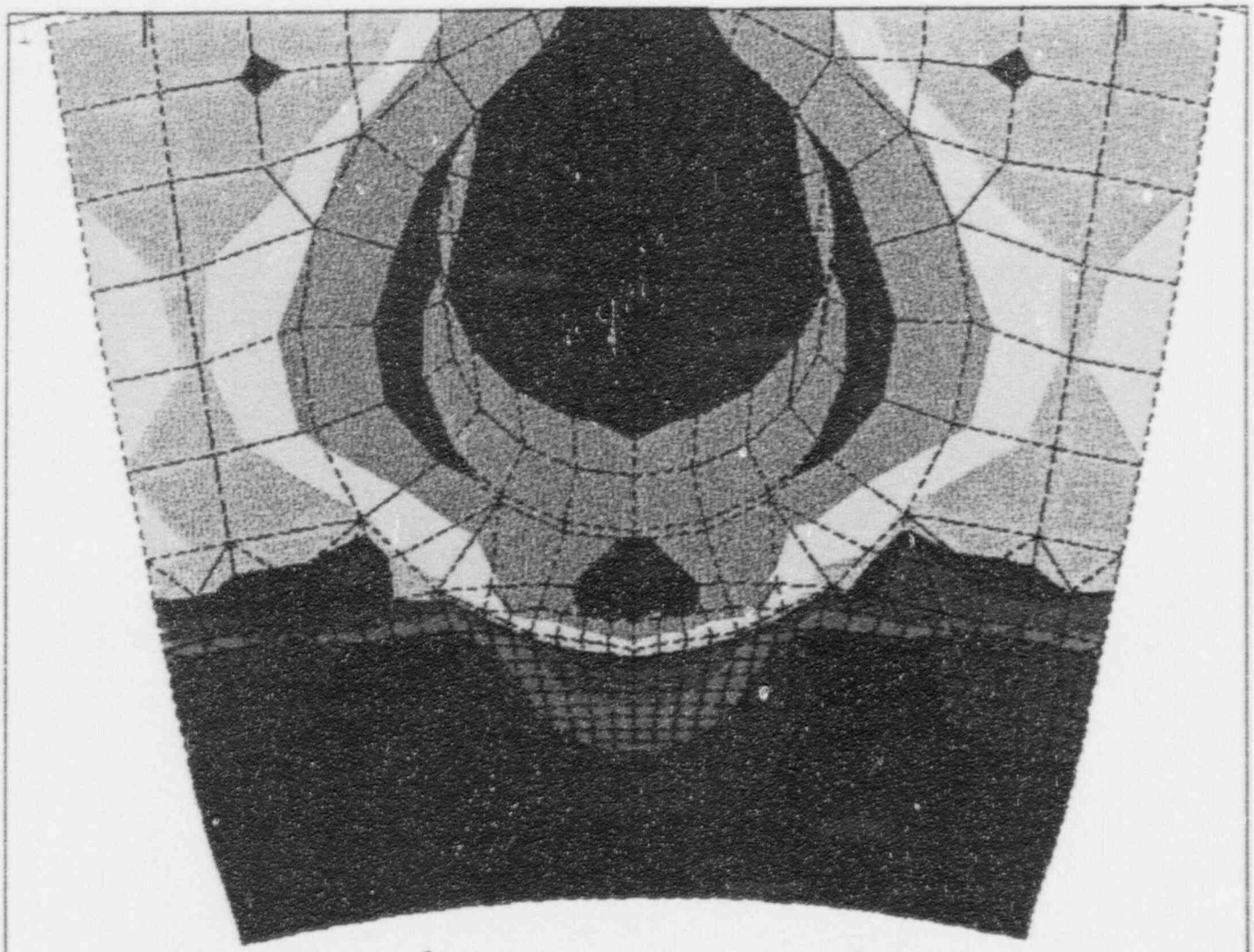


Figure 3-11 Lower Drywell Meridional Stresses - Refueling Case

OYSTER CREEK DRYWELL ANALYSIS - SYM-SYM, NOSAND, REFUELING

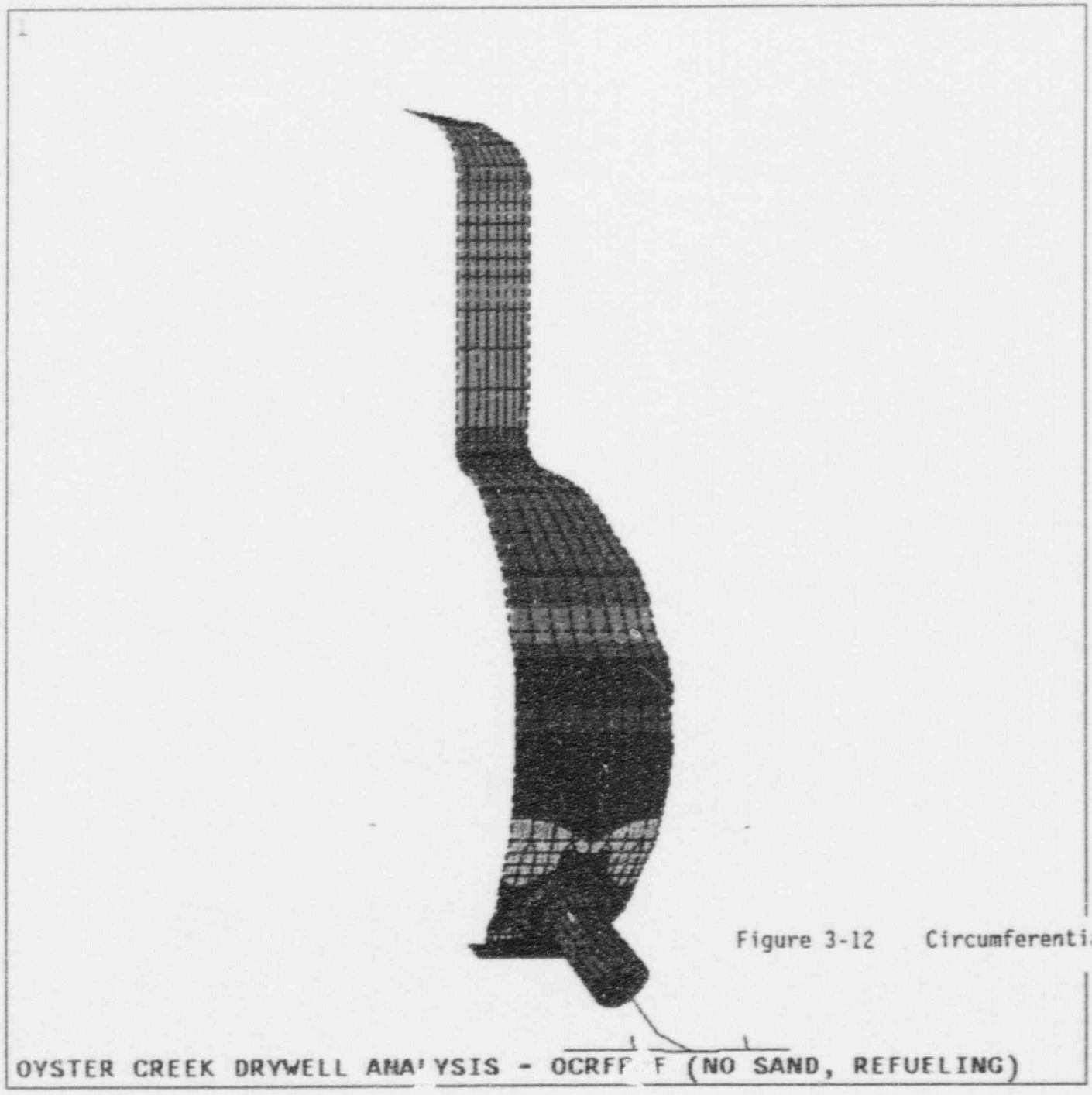


Figure 3-12 Circumferential Stresses - Refueling Case

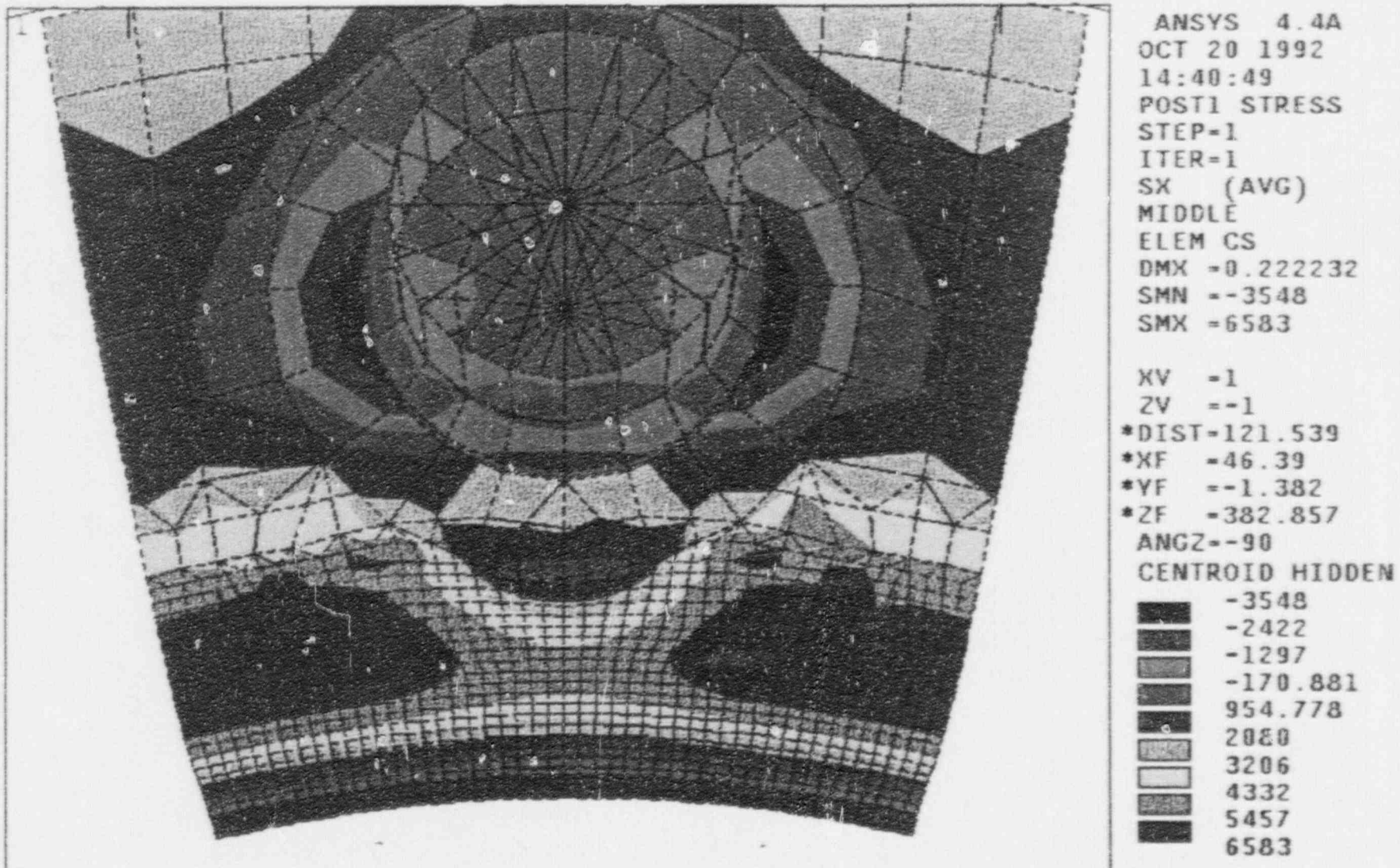


Figure 3-13 Lower Drywell Circumferential Stresses - Refueling Case

OYSTER CREEK DRYWELL ANALYSIS - SYM-SYM, NOSAND, REFUELING

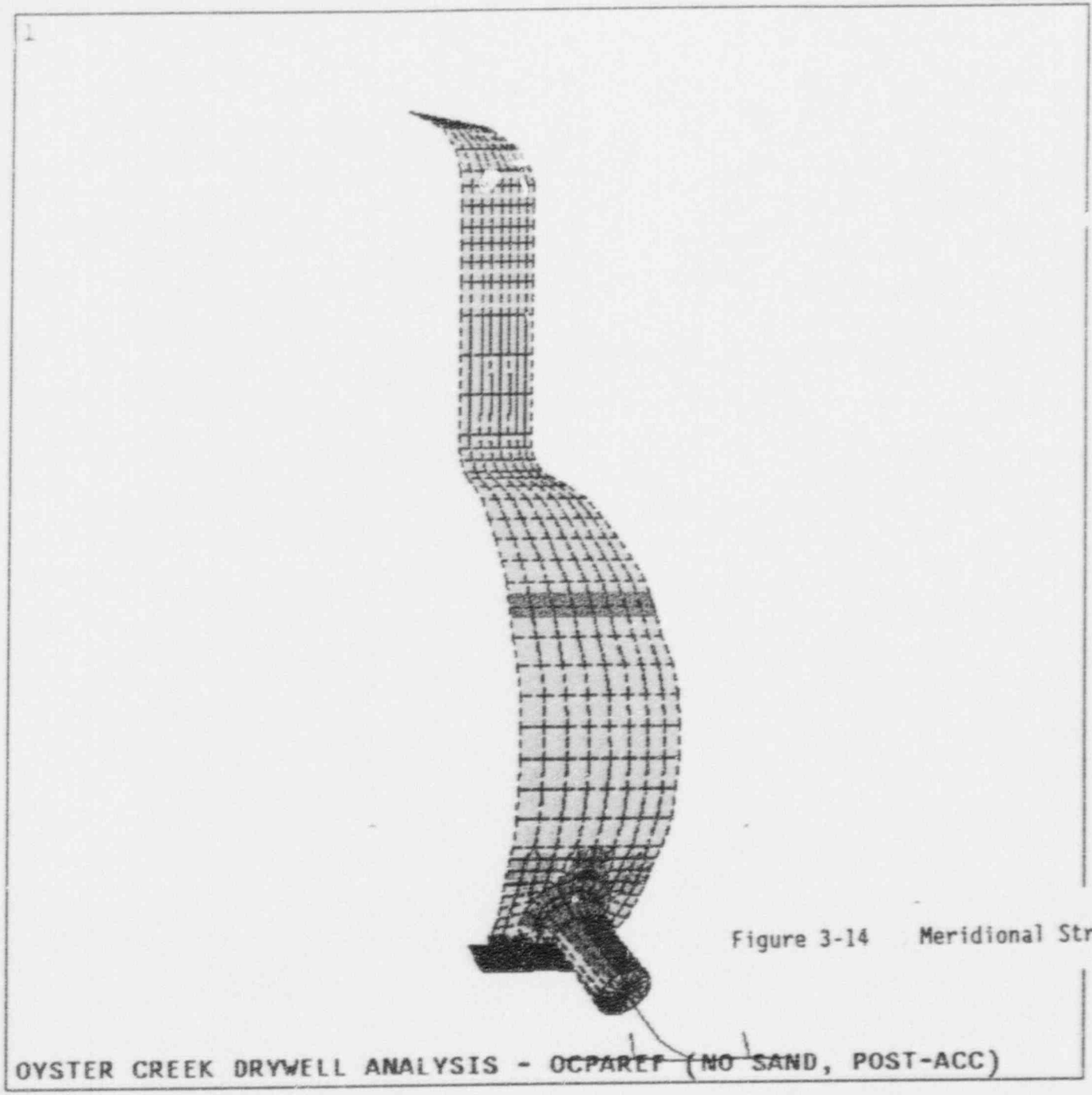


Figure 3-14 Meridional Stresses - Post-Accident Case

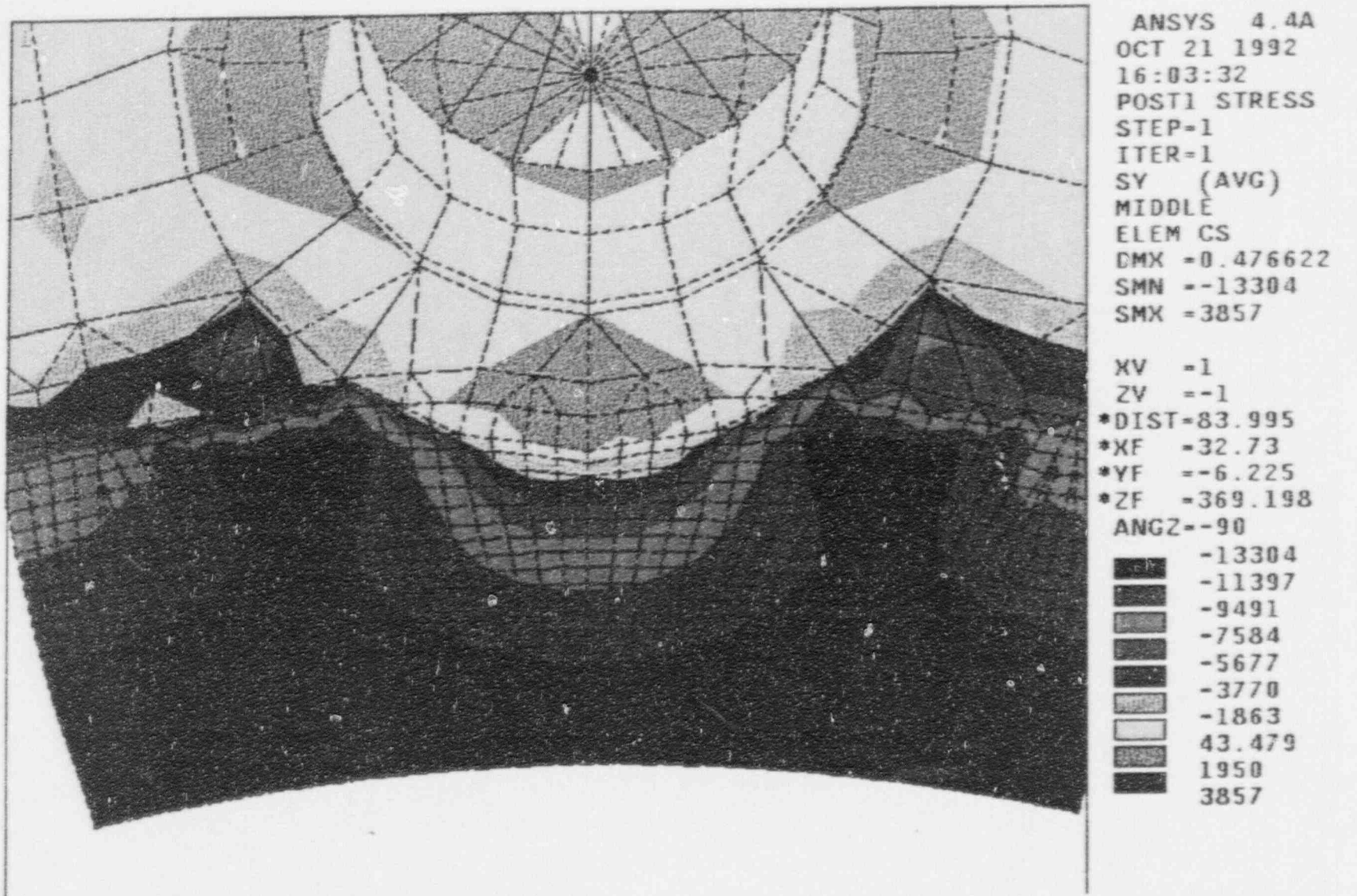


Figure 3-15 Lower Drywell Meridional Stresses - Post-Accident Case

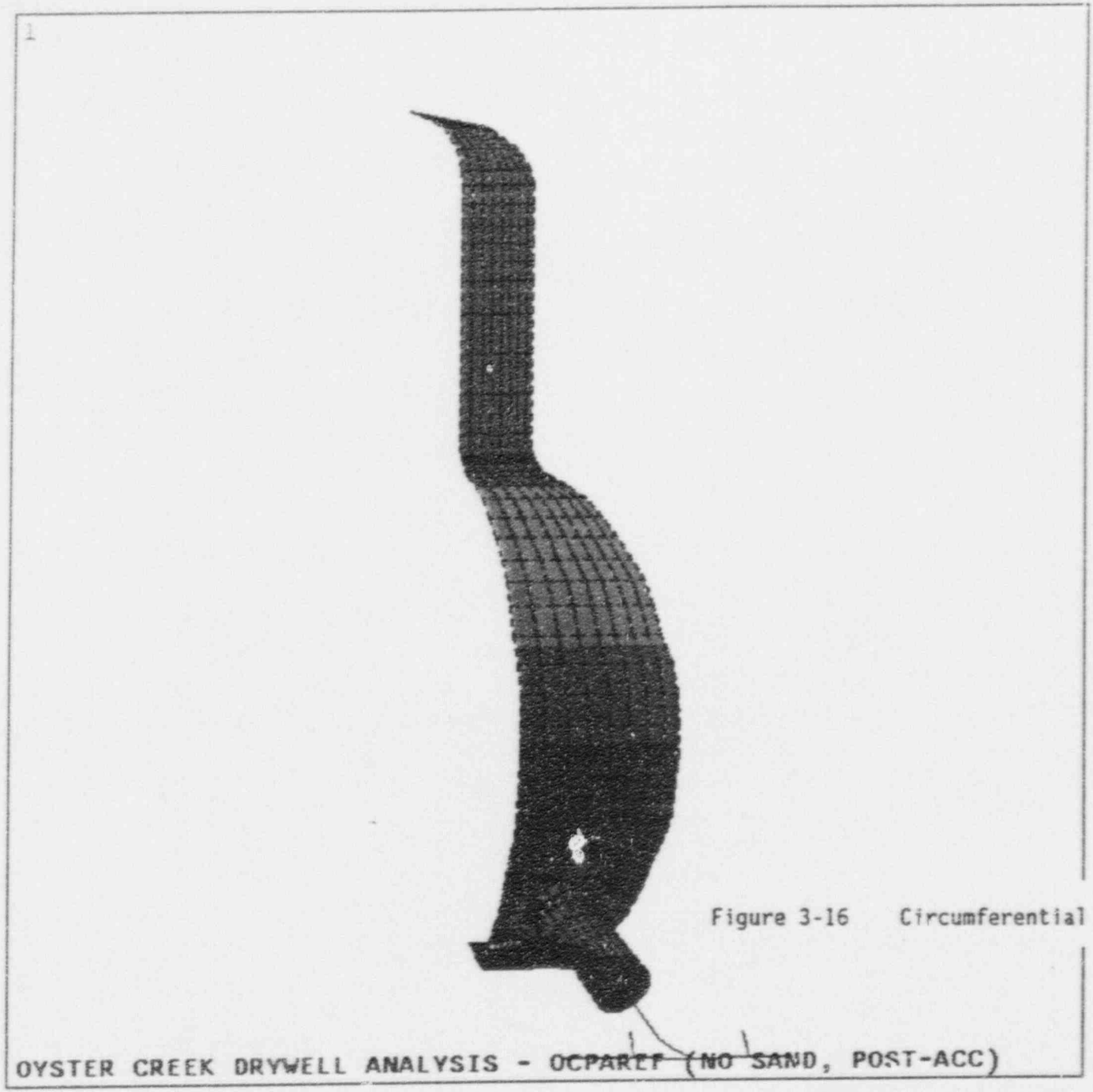


Figure 3-16 Circumferential Stresses - Post-Accident Case

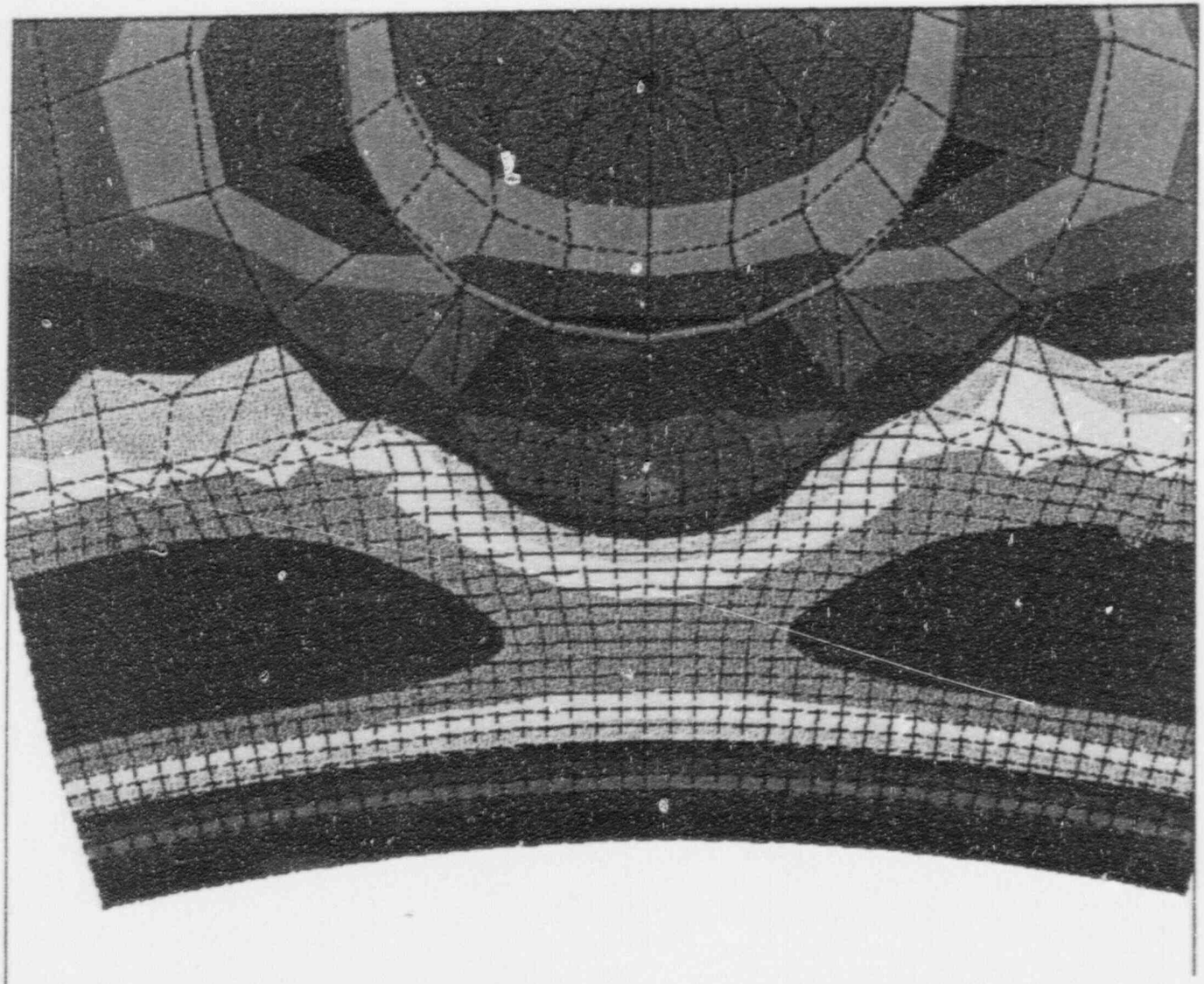


Figure 3-17 Lower Drywell Circumferential Stresses - Post-Accident Case

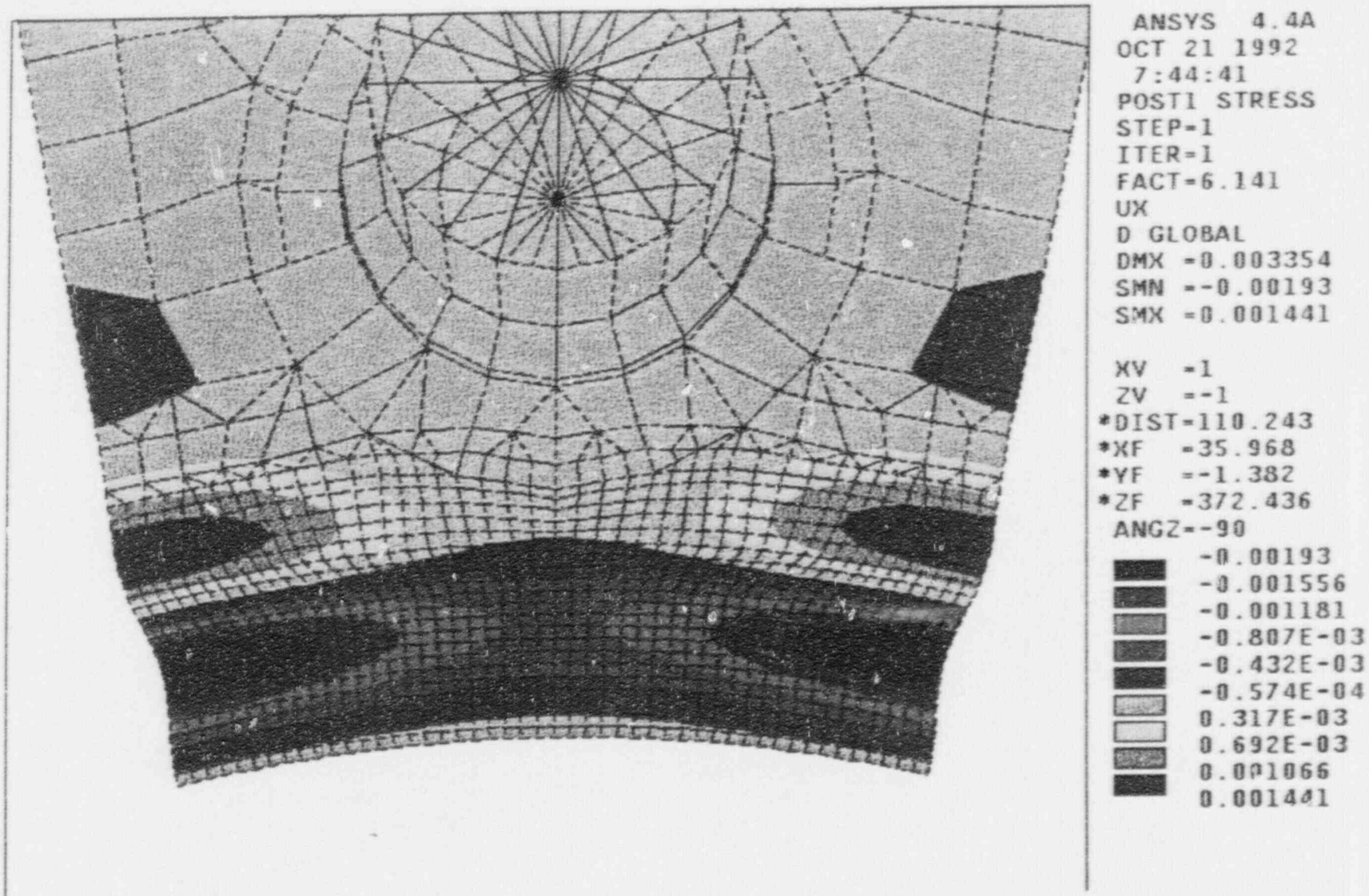


Figure 3-18 Sym-Sym Buckling Mode Shape - Refueling Case

OYSTER CREEK DRYWELL ANALYSIS - OCRFREF SYM-SYM (NO SAND, REFUELING)

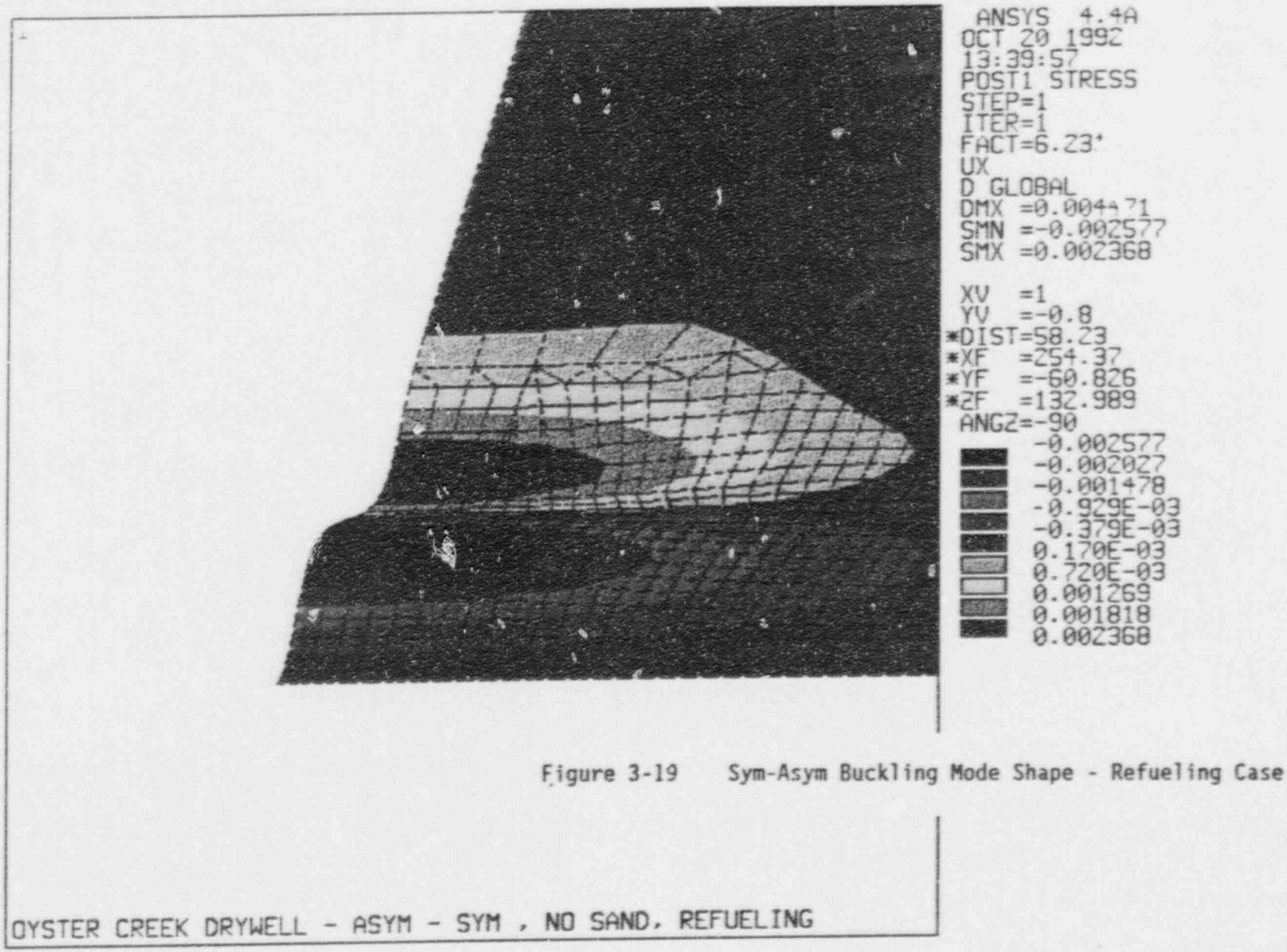


Figure 3-19 Sym-Asym Buckling Mode Shape - Refueling Case

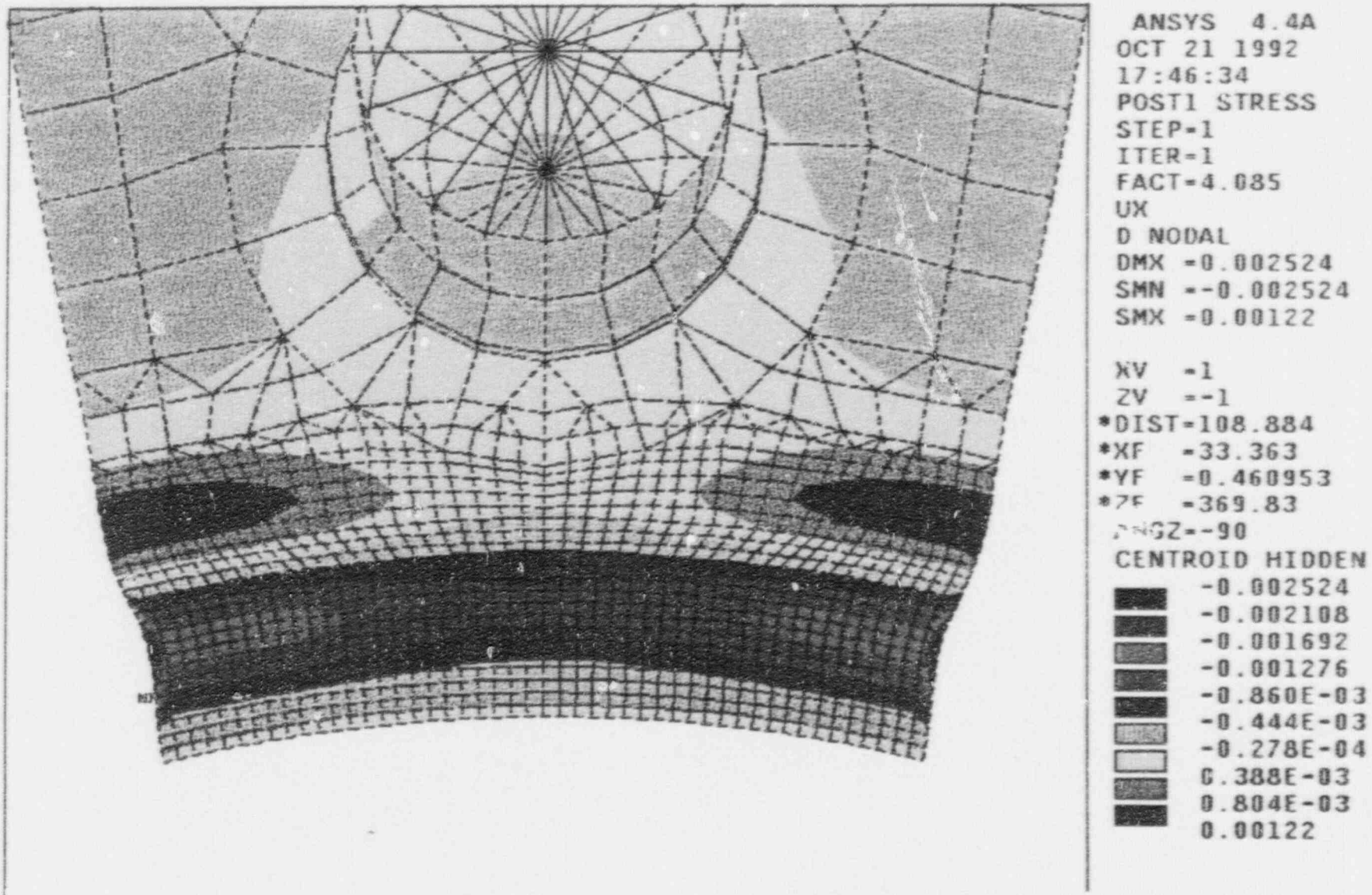


Figure 3-20 Sym-Sym Buckling Mode Shape - Post Accident Case

OYSTER CREEK DRYWELL ANALYSIS, OCPARFBK, SYM-SYM, NO SAND

# 4. ALLOWABLE BUCKLING STRESS EVALUATION

Applying the methodology described in Section 2 for the modification of the theoretical elastic buckling stress, the allowable compressive stresses are now calculated. Tables 4-1 and 4-2 summarize the calculation of the allowable buckling stresses for the Refueling and Post-Accident conditions, respectively. The modified capacity reduction factors are first calculated as described in sections 2.2 and 2.3. After reducing the theoretical instability stress by this reduction factor, the plasticity reduction factor is calculated and applied. The resulting inelastic buckling stresses are then divided by the factor of safety of 2.0 for the Refueling case and 1.67 for the Post-Accident case to obtain the final allowable compressive stresses.

The allowable compressive stress for the Refueling case is 7.59 ksi. Since the applied compressive stress is also 7.59 ksi, it indicates that the safety factor is equal to the Code required value of 2.0. The calculated allowable value of 7.59 ksi is conservative since the knockdown factors were calculated conservatively and a uniformly corroded thickness of sandbed is assumed. The allowable compressive stress for the Post-Accident, flooded case is 12.93 ksi as compared to the applied compressive stress of 12.0 ksi. Therefore, for both cases, the drywell meets the required ASME Code safety factors.

Table 4-1

Calculation of Allowable Buckling Stresses - Refueling Case

| Parameter | Value |
|---|---|
| Theoretical Elastic Instability Stress, $\sigma_{ie}$ (ksi) | 46.59 |
| Capacity Reduction Factor, $\alpha_i$ | 0.207 |
| Circumferential Stress, $\sigma_c$ (ksi) | 4.51 |
| Equivalent Pressure, p (psi) | 15.81 |
| "X" Parameter | 0.087 |
| $\Delta C$ | 0.072 |
| Modified Capacity Reduction Factor, $\alpha_{i,mod}$ | 0.326 |
| Elastic Buckling Stress, $\sigma_e = \alpha_{i,mod}\ \sigma_{ie}$ (ksi) | 15.18 |
| Proportional Limit Ratio, $\Delta = \sigma_e / \sigma_y$ | 0.40 |
| Plasticity Reduction Factor, $\eta_i$ | 1.00 |
| Inelastic Buckling Stress, $\sigma_i = \eta_i\ \sigma_e$ (ksi) | 15.18 |
| Code Factor of Safety, FS | 2.0 |
| Allowable Compressive Stress, $\sigma_{all} = \sigma_i/FS$ (ksi) | 7.59 |
| Applied Compressive Meridional Stress, $\sigma_m$ (ksi) | 7.59 |

Table 4-2

Calculation of Allowable Buckling Stresses - Post-Accident Case

| Parameter | Value |
|---|---|
| Theoretical Elastic Instability Stress, $\sigma_{ie}$ (ksi) | 49.020 |
| Capacity Reduction Factor, $\alpha_i$ | 0.207 |
| Circumferential Stress, $\sigma_c$ (ksi) | 20.21 |
| Equivalent Pressure, p (psi) | 70.84 |
| "X" Parameter | 0.39 |
| $\Delta C$ | 0.183 |
| Modified Capacity Reduction Factor, $\alpha_{i,mod}$ | 0.509 |
| Elastic Buckling Stress, $\sigma_e = \alpha_{i,mod}\ \sigma_{ie}$ (ksi) | 24.94 |
| Proportional Limit Ratio, $\Delta = \sigma_e / \sigma_y$ | 0.656 |
| Plasticity Reduction Factor, $\eta_i$ | 0.866 |
| Inelastic Buckling Stress, $\sigma_i = \eta_i\ \sigma_e$ (ksi) | 21.59 |
| Code Factor of Safety, FS | 1.67 |
| Allowable Compressive Stress, $\sigma_{all} = \sigma_i/FS$ (ksi) | 12.93 |
| Applied Compressive Meridional Stress, $\sigma_m$ (ksi) | 12.0 |

# 5. SUMMARY AND CONCLUSIONS

The results of this buckling analysis for the refueling and post-accident load combinations are summarized in Table 5-1. The applied and allowable compressive meridional stresses shown in Table 5-1 are for the sandbed region which is the most limiting region in terms of buckling. This analysis demonstrates that the Oyster Creek drywell has adequate margin against buckling with no sand support for an assumed sandbed shell thickness of 0.736 inch. This thickness is the 95% confidence projected thickness for the 14R outage. Therefore, for both cases, the drywell meets the required ASME Code safety factors.

Table 5-1

Buckling Analysis Summary

| | Load Combination | |
|---|---|---|
| | Refueling | Post-Accident |
| Service Condition | Design | Level C |
| Factor of Safety Applied | 2.00 | 1.67 |
| Applied Compressive Meridional Stress (ksi) | 7.59 | 12.0 |
| Allowable Compressive Meridional Stress (ksi) | 7.59 | 12.93 |
| Actual Buckling Safety Factor | 2.00 | 1.80 |